Ocean Engineering 36 (2009) 873–890

Contents lists available at ScienceDirect

Ocean Engineering

journal homepage: www.elsevier.com/locate/oceaneng

Modelling and observation of oscillatory sheet-flow sediment transport

J. Malarkey [a,*], S. Pan [b], M. Li [c], T. O'Donoghue [d], A.G. Davies [a], B.A. O'Connor [c]

[a] School of Ocean Sciences, Bangor University, Menai Bridge, Anglesey, LL59 5AB, UK
[b] School of Engineering, University of Plymouth, Drake Circus, Plymouth, PL4 8AA, UK
[c] Department of Engineering, University of Liverpool, Brownlow Street, Liverpool, L69 3GQ, UK
[d] School of Engineering, University of Aberdeen, King's College, Aberdeen, AB24 3UE, UK

ARTICLE INFO

Article history:
Received 23 September 2008
Accepted 6 May 2009
Available online 15 May 2009

Keywords:
Sediment transport
Modelling
Waves
Oscillatory sheet-flow
Asymmetric (velocity-skewed)
Experiments

ABSTRACT

Sand transport beneath large waves occurs in the plane-bed, sheet-flow regime. Comparisons between two sediment transport models and oscillatory sheet-flow experiments conducted in a flow tunnel are presented here. The experiments represent field-scale asymmetric (velocity-skewed) wave conditions over fine, medium and coarse sands, with median grain diameters of 0.13, 0.27 and 0.46 mm, respectively. The two numerical models used in the study are a two-phase flow model and a simpler two-layer, turbulence-closure model, both of which are one-dimensional vertical (1DV). The two-phase model takes account of the complete fluid–particle interactions, and the two-layer model uses an empirical description of the processes within the sheet-flow layer. The measured and predicted time-varying velocity, concentration and flux profiles, as well as the erosion depth and the net transport rates are compared and analysed. Overall, the predictions of both models are shown to be in good agreement with the measurements. The models predict the changing characteristics of the sheet-flow layer with grain size including the increasing importance of phase-lag effects for finer sands and the change in the net transport rate direction from onshore for coarse and medium sands to offshore for fine sands, with important implications for sediment sorting in the nearshore zone.

1. Introduction

Oscillatory sheet-flow conditions occur above plane beds when wave-generated, near-bed flow velocities are high, for example, under storm waves (Osborne and Vincent, 1993). Here, a significant portion of the sand is transported within a thin fluid–sediment layer of the order of a centimeter thick close to the bed, where the collisional nature of the sediment becomes important (Janssen et al., 1997). The magnitude of net sediment transport under sheet-flow conditions is typically very large and it can have a considerable impact on the overall transport budget in the nearshore zone (de Leeuw, 2005). For this reason, oscillatory sheet flows have been studied intensively in the past decade using both experiments and numerical models.

Experimental research on oscillatory sheet flow has been conducted in facilities, such as the Large Oscillating Water Tunnel (LOWT) at Delft Hydraulics (Ribberink and Al-Salem, 1995; Dohmen-Janssen, 1999; McLean et al., 2001), the Aberdeen Oscillatory Flow Tunnel (AOFT) at Aberdeen University (O'Donoghue and Wright, 2004a, b) and the Large Wave Flume or Grossen Wellenkanal (GWK) at FZK in Hanover (Dohmen-Janssen and Hanes, 2002). The most detailed measurements of sheet-flow processes – time-varying velocities, concentrations, erosion depths – have been obtained from AOFT experiments involving a range of sand sizes and symmetric and asymmetric (velocity-skewed) oscillatory flows. It is acknowledged that tunnels provide an approximation to the flow experienced at the seabed under real waves and that differences in the detailed near-bed hydrodynamics between tunnel flows and real waves are potentially important in determining net sediment transport rates (Dohmen-Janssen and Hanes, 2002). However, the number of sheet-flow experiments under real waves is very limited, with insufficiently detailed measurements of sheet-flow layer velocities and concentrations. Moreover, oscillatory tunnel experiments provide an ideal means of testing numerical models without the complication of the free surface.

A range of numerical models has been developed for oscillatory sheet-flow conditions. The models vary widely in their complexity from process-based, two-phase flow models (Asano, 1990; Li and Sawamoto, 1995; Dong and Zhang, 2002; Calantoni et al., 2004; Li et al., 2008; Liu and Sato, 2006; Amoudry et al., 2008), which represent the full diffusive and collisional nature of the process, to more empirically based models (Davies et al., 1997; Davies and Li, 1997; Rose et al., 1999; Guizien et al., 2003), which typically represent the transport process as purely diffusive and describe the sheet-flow layer only via a bedload transport formula. A compromise between these two extremes in complexity is represented by the models of Kaczmarek and Ostrowski

* Corresponding author. Tel.: +44 1248382848; fax: +44 1248716367.
E-mail address: j.malarkey@bangor.ac.uk (J. Malarkey).

0029-8018/$ - see front matter
doi:10.1016/j.oceaneng.2009.05.003

Nomenclature

A_1	1st harmonic orbital amplitude ($=U_1/\omega$)
D	grain diameter
T	flow period
U_1	1st harmonic free-stream velocity amplitude
U_2	2nd harmonic free-stream velocity amplitude
$U_{\max}$	maximum free-stream velocity ($=U_1+U_2$)
c	concentration
c_0	stationary bed concentration ($=0.6$)
c_δ	concentration at top of sheet-flow layer ($=0.08$)
d_0	orbital diameter ($\approx 2[U_1^2+U_2^2]^{0.5}/\omega$)
e	2.7182818
g	gravitational acceleration
i	$(-1)^{1/2}$
k	turbulent kinetic energy
k_s	roughness
s	sediment specific gravity
t	time
u	horizontal velocity
u_1, u_2	complex 1st and 2nd harmonic of velocity
u_∞	free-stream velocity
$\langle q\rangle$	best estimate of net transport rate
$\Delta\langle q\rangle$	error in net transport rate
$\langle q_m\rangle$	net transport rate from mass conservation
$\langle q_{\mathrm{i}}\rangle$	net transport rate from integration
z	vertical coordinate relative to undisturbed bed
z_0	$k_s/30$
β	length scale of CCM characterisation
δ	sheet-flow layer thickness
$\delta_{\min}$, δ_δ and γ	constants used in defining δ for UB model
ε	turbulent kinetic energy dissipation rate
ζ	erosion depth
θ	Shields parameter
π	3.1415927
ω	angular frequency ($=2\pi/T$)
$\langle\ldots\rangle$	cycle mean e.g. $\langle u\rangle$
Re	real part of a complex quantity e.g. $\mathrm{Re}\{u_1\}$
$\lvert\ldots\rvert$	magnitude of a complex quantity e.g. $\lvert u_1\rvert$
arg	phase of a complex quantity e.g. $\arg(u_1)$

(2002) and Malarkey et al. (2003), in which the sheet-flow layer is prescribed more realistically.

Unlike the two-phase models, the diffusion-type models and the models of Kaczmarek and Ostrowski (2002) and Malarkey et al. (2003) all rely on the key assumption of quasi-steadiness, which forces the instantaneous stress to be linked to the instantaneous sheet-flow layer thickness and transport in this layer. A major drawback to this type of simple model is the neglect of the delay in response time of the sediment, the so-called phase-lag effect in the sheet-flow layer (see Dohmen-Janssen et al., 2002). Phase-lag effects become increasingly important as the sediment becomes finer, with the result that quasi-steady models tend to produce poorer predictions for fine sands.

This paper is based on research carried out within the 'LUBA' project, involving the Universities of Liverpool, Bangor and Aberdeen in the UK. It presents a detailed intercomparison of two models of differing complexity with experimental data from an oscillatory flow tunnel. The two models, which are both one-dimensional vertical (1DV) to represent tunnel conditions, are the two-phase model of Li et al. (2008) developed at the University of Liverpool (UL) and an updated version of the two-layer 1DV model of Malarkey et al. (2003) developed at the University of Bangor (UB). The updated UB model has a more realistic description of the sheet-flow layer and includes a parameterised phase-lag effect. The models are compared with data from the sheet-flow experiments of O'Donoghue and Wright (2004a, b) and Li et al. (2003) carried out in the AOFT. The detailed and complete nature of the measurements, over a range of grain sizes, also allows comparisons at every step with model output (velocity, concentration and flux) to critically test the models and track any differences through to the final net transport rate. The experiments and models are described in Sections 2 and 3 of the paper, respectively. The intercomparison between models and experimental results is presented in Section 4 and is discussed in Section 5. The main conclusions are presented in Section 6.

2. Experiments

The present paper is based on a subset of the 22 sheet-flow experiments reported by O'Donoghue and Wright (2004a, b) and four new LUBA experiments, reported on by Li et al. (2003). All of the experiments were carried out in the AOFT, which is a large laboratory facility capable of producing horizontal oscillatory flows with periods and amplitudes equivalent to those of near-bed oscillatory flows generated by full-scale waves in the field. Oscillatory flows with field-scale periods and amplitudes mean that the scale effects associated with experiments in smaller laboratory facilities are avoided. The AOFT has a U-tube construction with an overall length of 16 m. The 10 m long, glass-sided test section is 0.75 m high and 0.3 m wide. For the experiments reported here, a 0.25 m deep sand bed occupied the test section, leaving 0.5 m for the flow above. During each experiment, the net transport rate was calculated by applying the mass conservation principle to the pre- and post-experiment bed profiles together with the masses of sand collected from the two ends of the test section.

A range of equipment was used to measure sediment concentrations and velocities during the experiments. Time-varying sediment concentrations within the sheet-flow layer were measured using two conductivity concentration meters (CCMs). Each CCM provided the concentration at one height, sampled at 50 Hz and recorded over 12 flow cycles. The CCM probes had an elevation that was adjustable and could be located to an accuracy of ± 0.05 mm. Time-varying concentrations in the suspension layer were measured by eight suction samplers connected to a carousel type collector. The eight suction samplers each provided concentration at a given height 20 times per flow cycle that were phase ensembled over 20 flow cycles. The particle sizes for the suspended and transported sands were determined by a laser diffraction particle size analyser (see O'Donoghue and Wright, 2004b). For the LUBA experiments, a high-resolution acoustic backscatter system (ABS) was used to measure time-varying sediment concentrations in the suspension layer. The ABS provided 128 measurements of concentrations in the vertical with a resolution of 2.5 mm and a sampling frequency of 128 Hz, which were typically phase ensembled over 10–12 flow cycles (Li et al., 2003).

The sediment concentration from the CCMs within the sheet-flow layer was based on phase ensembling composite CCM readings from many repeat experiments that continuously accounted for the change in the undisturbed bed level during the course of the experiment (see O'Donoghue and Wright, 2004a). The method used yielded accurate determination of two important parameters involved in sheet-flow analysis: the erosion depth $\zeta(t)$ and the sheet-flow layer thickness $\delta(t)$, as shown in

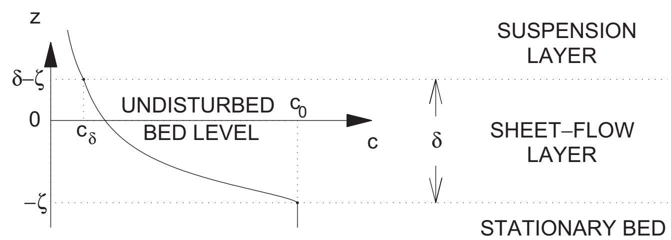

Fig. 1. Schematic of instantaneous concentration profile, where $c_0 = 0.6$ and $c_\delta = 0.08$.

Fig. 1. The time-varying erosion depth $\zeta(t)$ is defined as the distance from the initial undisturbed bed level ($z = 0$) down to the position where the volumetric concentration reaches its stationary bed value c_0 (measured to be 60%) and the top of the sheet-flow layer is defined as the position where volumetric concentration is equal to c_δ (taken here as 8%). The choice of $c_\delta = 8\%$ for the top of the sheet-flow layer has been used by other researchers (see for example Dohmen-Janssen et al., 2001) since it corresponds to median-sized grains being spaced approximately one grain diameter apart, such that granular interactions can reasonably be neglected. Thus, the time-varying, sheet-flow layer thickness is defined as the distance between elevations where the volumetric concentration is 8% and 60%. Typically, the 8% height occurred somewhere between the operating levels of the CCM probes and the suction-sample and ABS instruments. From their experiments, O'Donoghue and Wright (2004a) demonstrated that the CCM concentration measurements within the sheet-flow layer are well characterised by

$$c(z,t) = \frac{c_0}{1 + [(z + \zeta(t))/\beta(t)]^{1.5}}, \tag{1}$$

such that the concentration can be represented by the time-varying erosion depth $\zeta(t)$ and a function $\beta(t)$ that represents the vertical scale of the sheet-flow layer. The functions $\zeta(t)$ and $\beta(t)$ in Eq. (1) are found by least-squares-fitting to the CCM data. This characterisation is also useful, as will be shown later, because the CCM measurements become quite noisy near the top of the sheet-flow layer.

Time-varying vertical profiles of velocity from the outer suspension layer to deep within the sheet-flow layer were measured using an ultrasonic velocity profiler (UVP). The UVP provided 128 measurements of velocity with a 0.56 mm vertical spacing, a velocity resolution of 7.4 mm/s and a sampling frequency of 20 Hz. The velocity measurements were phase ensembled over 10 flow cycles and located relative to the mean undisturbed bed level (see O'Donoghue and Wright, 2004b). Velocity measurements were not carried out for all experimental conditions, but O'Donoghue and Wright found that the measured near-bed velocities for a given flow were not sensitive to the sand size and grading, at least for the size and grading ranges covered by their experiments. They concluded that velocities measured for one sand applied to the other sands also. Furthermore, O'Donoghue and Wright found that it was possible to measure velocities typically down to the undisturbed bed level ($z = 0$). Therefore, to determine the sand flux at any phase in the flow cycle, they assumed a linear velocity profile from the measured velocity at $z = 0$ down to zero velocity at the measured instantaneous erosion depth. It should be noted that the UVP measures sediment particle velocities, not fluid velocities. Based on two-phase flow modelling, Dong and Zhang (1999) and Li et al. (2008) showed that the expected difference between sand and fluid velocities within the sheet-flow layer is typically less than 0.5% of the free-stream velocity amplitude, rising to 2–2.5% near the undisturbed bed level ($z = 0$).

This paper focuses on six of the O'Donoghue and Wright (2004a, b) experiments and two of the LUBA experiments as detailed in Table 1. The six O'Donoghue and Wright experiments involve three well-sorted sands – 'fine' with $D = 0.13$ mm, 'medium' with $D = 0.27$ mm and 'coarse' with $D = 0.46$ mm – in two flows with $T = 5$ s and $T = 7.5$ s; the two LUBA experiments involve the fine sand in two flows with $T = 4$ and 6 s. The target free-stream velocity for each experiment was asymmetric and given by

$$u_\infty(t) = U_1 \cos(\omega t - \alpha) + U_2 \cos 2(\omega t - \alpha), \tag{2}$$

where positive $u_\infty(t)$ is 'onshore' directed, t time, $\omega = 2\pi/T$, T the oscillatory flow period, U_1 and U_2 are the first and second harmonic amplitude of the velocity and α is given by

$$\alpha = \arccos\left[\frac{\sqrt{U_1^2 + 8U_2^2} - U_1}{U_2}\right]. \tag{3}$$

The values of U_1 and the flow asymmetry, U_2/U_1, listed in Table 1 were determined from time-series at the uppermost UVP measurement position ($z = 40$ mm). The measured maximum velocities, $U_{\max}$, ($= U_1+U_2$) were typically found to be 10% smaller than those derived from the movement of the tunnel's piston, see for example O'Donoghue and Wright (2004a). The free-stream velocity given by Eq. (2) is illustrated in Fig. 2 (the numbered lines indicate the phases referred to later in the results section). This asymmetric free-stream velocity gives rise to a cycle-mean velocity profile which has a zero depth average, because the AOFT cannot support a net current through the tunnel.

3. Model descriptions

3.1. UL two-phase model

The 1DV, two-phase model of Li et al. (2008) (herein called the "UL" model) uses the continuity and momentum equations for both fluid and sediment phases as presented by Dong and Zhang (1999) and Hsu et al. (2003). In addition to sediment and fluid shear stresses, the model includes: drag and lift forces resulting

Table 1
AOFT asymmetric flow conditions where U_1 and U_2 are based on the uppermost UVP measurements (at 40 mm above the undisturbed bed level).

Test	D (mm)	T (s)	U_1 (m/s)	U_2/U_1 (−)
FA5010[a]	0.13	5.0	1.06	0.22
FA7515[a]	0.13	7.5	1.12	0.19
MA5010[a]	0.27	5.0	1.06	0.22
MA7515[a]	0.27	7.5	1.12	0.19
CA5010[a]	0.46	5.0	1.06	0.22
CA7515[a]	0.46	7.5	1.12	0.19
LA406	0.13	4.0	0.95	0.25
LA612	0.13	6.0	1.12	0.25

[a] Corresponds to tests undertaken by O'Donoghue and Wright (2004a, b).

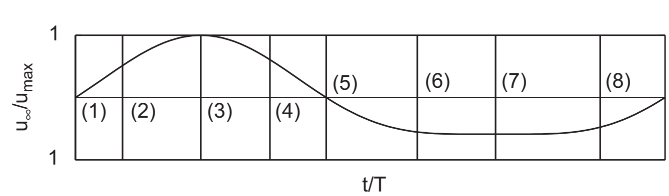

Fig. 2. Free-stream velocity for asymmetric flow (phases are numbered for later presentation of the results.)

from the relative sediment–fluid velocities; added mass forces resulting from the relative sediment–fluid accelerations and intergranular stresses based on Ahilan and Sleath's (1987) description. The model represents the turbulent kinetic energy distribution in the sand–fluid mixture in the sheet-flow and suspension layers using a k turbulence closure scheme. The turbulent kinetic energy dissipation rate is a function of the turbulent kinetic energy and sediment concentration. In the lower part of the sheet-flow layer (where $c>0.5c_0$), it is assumed that turbulence generation is dominated by inter-particle collisions and the turbulence length scale is therefore set to be proportional to the grain diameter. Higher in the flow (where $c\leqslant 0.5c_0$), a free turbulence region following a conventional one-equation closure is assumed, in which the turbulence length scale is proportional to the distance from the level where $c=0.5c_0$ (typically corresponding to just below the undisturbed bed level, $z=0$). Based on the conservation equations of mass, momentum and turbulent kinetic energy, the model is able to predict vertical profiles of velocity, for both the fluid and sediment phases, as well as sediment concentration from the stationary bed up to the top of the water column. The computational grid, which has a fixed cell size, typically extends a further 1.5 cm below the expected position of the time-varying erosion depth. The model is driven by a pressure gradient with a time-varying part determined by $\mathrm{d}u_\infty/\mathrm{d}t$, from Eq. (2), and a steady part to allow matching onto the outer most cycle-mean velocity measurement. The upper boundary condition was combined with a no-slip boundary condition at the base of the grid for both the fluid and sediment phases. At the upper boundary, the shear stresses, sediment flux and the gradient of k are all forced to be zero, and at the base of the grid, $c=c_0$ and $k=0$. It should be pointed out that below the erosion depth, defined here as the depth where $c=0.99c_0$, the eddy viscosity is zero and, because of the large stresses, there is negligible movement of sediment. The model was tested extensively against a symmetric fine-grained AOFT case (LS612, see Table B1) to determine the relevant coefficients, such as those for the collisional and lifting processes. It was found that a vertical grid resolution comparable to the grain diameter was required near the stationary bed level to give satisfactory model results for 9600 time steps per flow cycle. The computational effort required for such fine resolution was very demanding. To keep the computational time within a reasonable range, the domain was limited to the top of the wave boundary layer (corresponding to 960 cells in the vertical in total), but this was still sufficient to represent the processes fully. Further details of the model can be found in Li et al. (2008).

3.2. UB two-layer model

The UB model is a modification of the 1DV, two-layer model of Malarkey et al. (2003) for sheet-flow sand transport under wave and wave-plus-current conditions. The basic features of the model, which remain unchanged, are summarised below. The model separates the water column into two distinct layers, a sheet-flow layer near the bed and a suspension layer higher in the flow. A standard diffusion model with a k-ε turbulence closure scheme is used to resolve the suspension layer (defined by $c\leqslant c_\delta$) numerically, based on a prescribed roughness length scale, z_0. The velocity and concentration in the sheet-flow layer (defined by $c_0\geqslant c\geqslant c_\delta$) are prescribed analytically. The velocity and concentration are matched to the numerical solution in the suspension layer at the interface between the two layers where $z=\delta(t)-\zeta(t)$, as shown schematically in Fig. 3 ($u=u_\delta$ and $c=c_\delta$). Thus the method relies on the fact that there is an overlap between the upper numerical solution and the lower sheet-flow layer. The

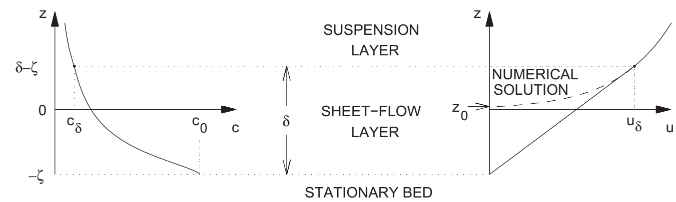

Fig. 3. Schematic of instantaneous sheet-flow and suspension layers in the UB model.

sheet-flow layer thickness, δ, is prescribed in terms of the instantaneous Shields parameter derived from the stress at the base of the outer solution. Conservation of sediment is satisfied by adjusting the erosion depth, ζ, at each time step, such that it is consistent with the total integrated sediment in the sheet-flow and suspension layers. The velocity profile in the sheet-flow layer is assumed to increase linearly from zero at the stationary bed level to the value determined by the outer-flow numerical solution at the top of the sheet-flow layer.

All of the changes made to the UB model in the present study are described in Appendix A; the most significant changes are in the treatment of the sheet-flow layer. In the sheet-flow layer, the updated model uses a prescribed concentration profile with the same functional form as proposed by O'Donoghue and Wright (2004a) (Eq. (1)), together with a sheet-flow layer thickness having the following time dependency:

$$\frac{\delta(t)}{D}=\delta_{\min}+\delta_\theta\theta(\omega t-\gamma), \tag{4}$$

where $\theta=u^{*2}/(s-1)gD$ is the instantaneous Shields parameter ($\theta\geqslant 0$), u^* is the time-varying friction velocity determined from stress at the base of the numerical outer-flow solution, s the relative density of the sediment, g the acceleration due to gravity and $\delta_{\min}$, δ_θ and γ are non-dimensional constants defined for particular oscillatory flow and sand conditions. The constants are parameterised in Appendix B (see Eqs. (B.4(a)–(c)) using results from AOFT symmetric flow experiments.

Inclusion of the more realistic concentration profile and the phase lag, γ, represent significant improvements to the original Malarkey et al. (2003) model. The phase-lag parameter allows the model to be freed from the constraint of the quasi-steady assumption which is particularly important in fine-grained cases where the delay in the response of the sheet-flow layer thickness to changes in the shear stress is typically between 25° and 45°.

4. Results

The models were run for each of the asymmetric flows listed in Table 1. Detailed discussion is focussed on the six asymmetric cases of O'Donoghue and Wright (2004a), to study the dependence of results on grain size and flow period. The two LUBA cases are included primarily for discussion of sediment fluxes and net transport rates. For each of the eight cases listed in Table 1, the models were driven by the measured free-stream velocity and matched to the cycle-mean velocity determined from the uppermost UVP measurement.

4.1. Consistency of the data

Before comparing the models and data, it is useful to consider the self consistency of the data. Fig. 4 shows the erosion depths for all the cases listed in Table 1. The erosion depth derived from Eq. (1), i.e. that based on the depth where concentration reaches its stationary bed value, is here compared with an erosion depth,

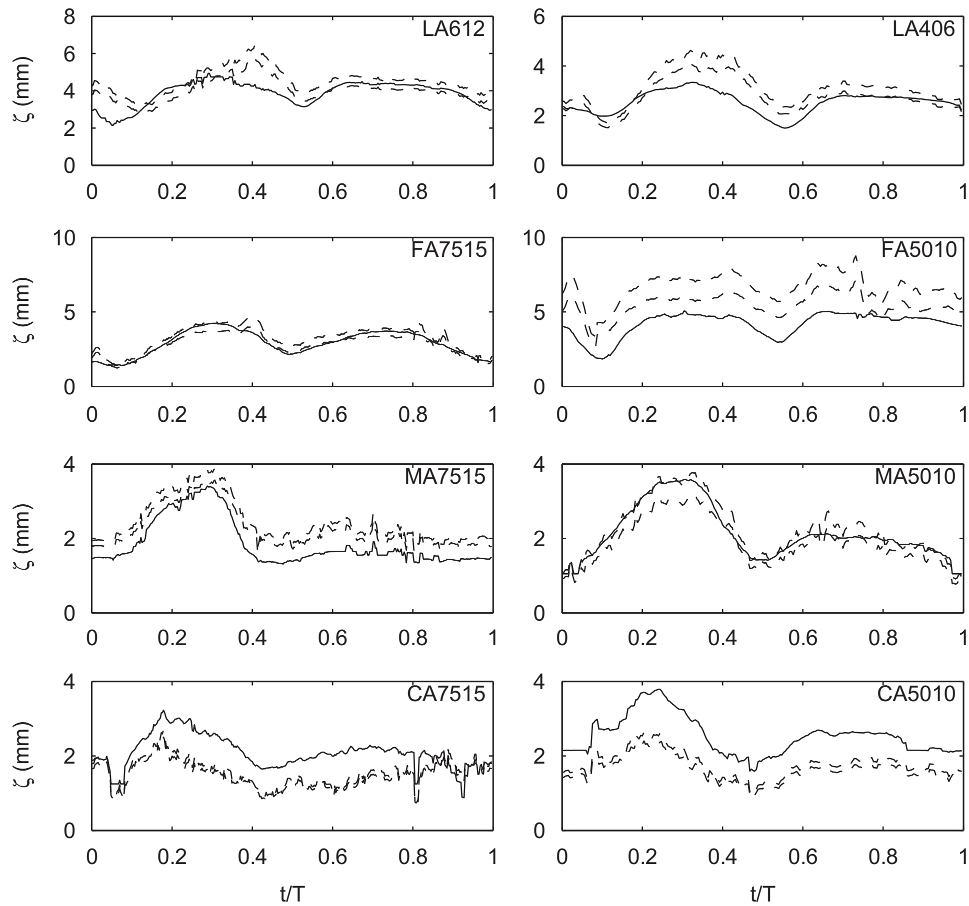

Fig. 4. Comparison of measured erosion depth (solid line) and erosion depth based on the integrated concentration profile divided by c_{0E} (dashed lines); there are two dashed lines corresponding to two values of c_{0E} (mean ± two standard deviations) in Eq. (4).

ζ_E, derived from integrating all of the CCM and suction-sample/ABS concentration measurements made above the erosion depth

$$\zeta_E c_{0E} = \int_{-\zeta}^{h} c\,\mathrm{d}z, \tag{5}$$

where h is the uppermost measurement height. Eq. (5) is an expression of the conservation of sediment concentration and c_{0E} is a measure of the stationary bed concentration. Since the concentration below the erosion depth can vary somewhat around its expected value (= 0.6), c_{0E} is defined as the mean ± two standard deviations of the concentration below the erosion depth, thus there are two values of ζ_E in Fig. 4. The data can be considered to be consistent if the solid line, ζ, lies between the two dashed lines of ζ_E. On the basis of this test, it can be seen that for three of the cases (FA7515, MA7515 and MA5010) there is remarkable consistency between the estimates. Two more cases (LA612 and LA406) are consistent for at least part of the cycle and when inconsistent, have ζ_E exceeding ζ by less than 1 mm. However, for the fine-grained test with $T = 5$ s (FA5010), ζ_E exceeds ζ by approximately 2 mm, and for the two coarse-grained tests (CA5010 and CA7515), ζ_E is less than ζ by approximately 1 mm. Thus, in the fine-grained case, there is apparently more sand suspended in the water column than the measured erosion depth implies and, in the two coarse-grained cases, there is less sand suspended than the measured erosion depth implies. It is unclear what the reason for the inconsistency might be.

It may be noted that the data can be similarly tested for consistency by integrating over all the measurement heights and then dividing by the magnitude of the lowest measurement height ($-z_1$) to produce another estimate of stationary bed concentration, c_{0E2}

$$c_{0E2} = \frac{1}{z_1}\int_{-z_1}^{h} c\,\mathrm{d}z. \tag{6}$$

If this value is always greater/less than the expected value of c_0 (= 0.6), then there must be too much/little sediment in the water column. The advantage of this approach is that it does not require the erosion depth to be located, only that $-z_1$ is always below the instantaneous erosion depth. Though not shown here, this test was found to produce inconsistency in the same three cases as those highlighted above. This should be borne in mind in the later discussion of the concentration comparisons since it is at odds with the two models which conserve concentration by definition. This issue of consistency, which is returned to in the discussion section, should not be interpreted as a criticism of the data which is actually remarkable for its detailed resolution of the key parameters in the sheet-flow layer.

4.2. Velocity

Fig. 5 shows a comparison between the predicted and measured profiles of velocity at six of the phases depicted in Fig. 2 for the tests with $T = 7.5$ and 5 s (A7515 and A5010) and the three grain sizes (F, M and C). Results from the two-phase UL model are sediment velocities, not fluid velocities. The linear profiles assumed in both the UB model, within the sheet-flow layer, and in the data, below the undisturbed bed level are clearly

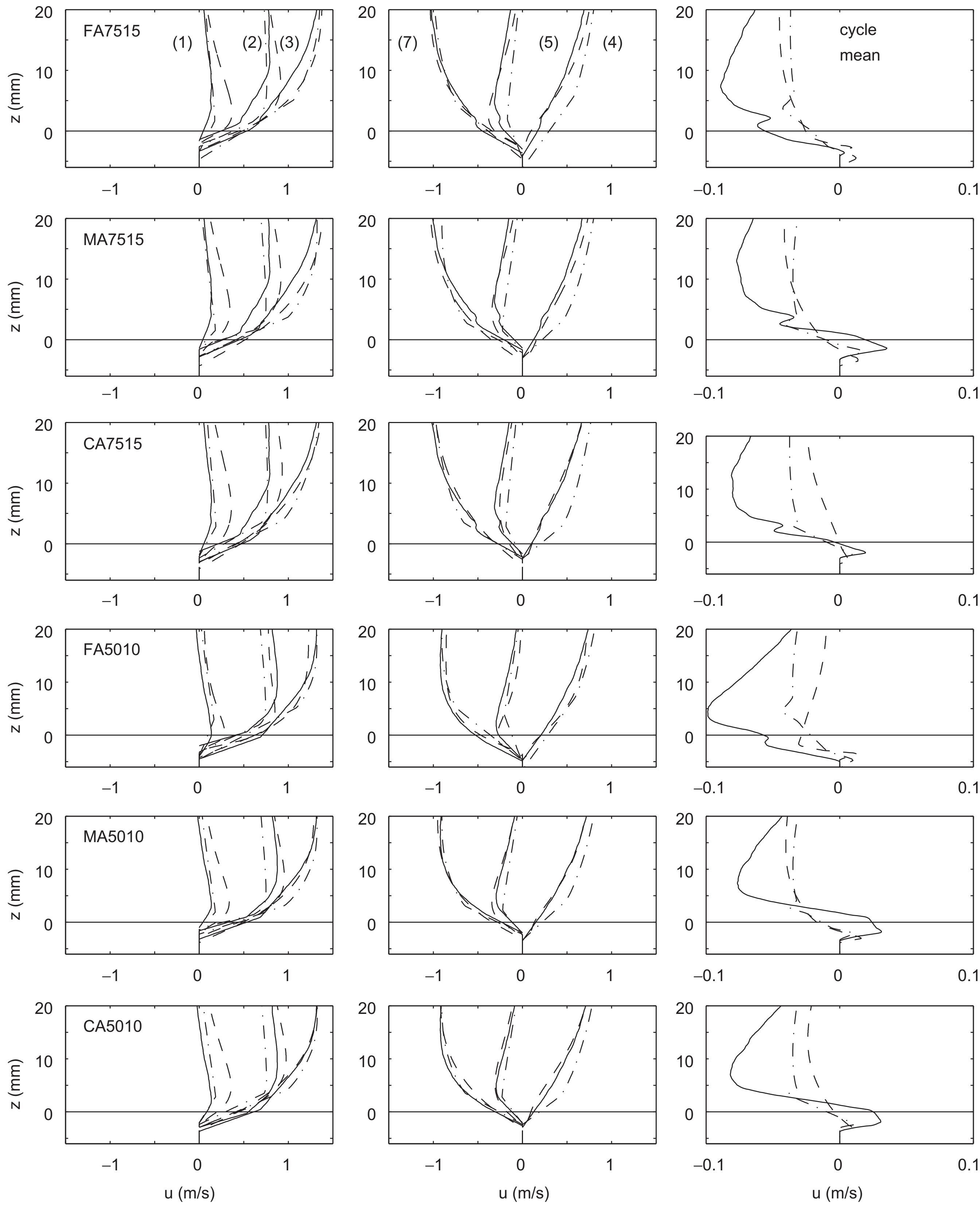

Fig. 5. Measured and predicted velocity profiles at phases 1, 2, 3, 4, 5 and 7 (see Fig. 2) and cycle-mean velocity profiles; two flows, A7515 and A5010, ($T = 7.5$ and 5 s) and three sands, F–, M– C– ($D = 0.13$, 0.27 and 0.46 mm). Solid line—measurement; dashed line—UL model; dashed–dotted line—UB model.

visible. Overall, there is generally good agreement between the models and the data for both flow periods and all three sand sizes. However, noticeable discrepancies between the predictions and the measurements are found for both models at two particular stages of the flow cycle. For the UL model, the largest differences occur during the accelerating phases [(1) and (2)], where the model results lead the data, while for the UB model the largest differences occur during the decelerating phases [(4) and (5)], where the model results lag behind the data. Both models agree well with the data at the phases of maximum free-stream velocity [(3) and (7)]. The reasons for the differences are unclear, but these results suggest that the eddy viscosity is not being correctly predicted in the two models at all phases. The cycle-mean velocity profiles are also shown in Fig. 5. In the outer sheet-flow and above the mean velocity is in the implied 'offshore' direction and occurs as a result of turbulence asymmetry in the two flow half cycles (see for example Davies and Li, 1997). Immediately above the stationary bed level, the mean flow is 'onshore' as a result of the larger velocities and deeper erosion depths in the onshore rather than the offshore half cycle. The models predict the basic structure of the cycle-mean profiles reasonably well but they substantially underpredict the magnitude of the offshore maximum in all six cases. For the near-bed onshore maximum, the models overpredict for the fine sand and underpredict for the medium and coarse sands. The profiles in Fig. 5 cover the bottom 4% of the water column in the tunnel (measurements actually cover the bottom 8% of the water column); net flow in one direction near the bed will be compensated for by a net flow in the other direction higher up in the water column.

To examine the phase behaviour more systematically, it is instructive to look also at the profiles of the harmonics of velocity in the wave boundary layer. Bearing in mind the free-stream velocity, Eq. (2), it is reasonable to expect that the boundary layer velocity can be represented by

$$u = \langle u \rangle + \mathrm{Re}\{u_1 e^{i\omega t} + u_2 e^{i2\omega t} + \cdots\}, \tag{7}$$

where $\langle u \rangle$ is the cycle-mean velocity, u_1 and u_2 are the complex first and second harmonics of velocity, Re denotes the real part and $i = (-1)^{1/2}$. Fig. 6 shows a comparison between the measured and predicted profiles of the amplitudes and phases of the velocity harmonics and the cycle-mean velocity profiles for the LA406 case; the results shown here are typical of all cases. The linear portion of the profile from the undisturbed bed level down to the erosion depth has been excluded from the data here to see the phase behaviour more clearly. Also, the harmonic profiles of the models only extend down as far as the shallowest erosion depth. The figure shows generally close agreement between the models and the data. The UB model appears to predict the position of the overshoot slightly better than the UL model, which may be because of the higher order turbulence closure used in the UB model – k-ε rather than k (Justesen, 1991). In this case, the UL model predicts the first harmonic phase better and the UB model predicts the second harmonic phase better. The phases do not tend to zero far above the bed because of the free-stream definition, see Eq. (2). It is interesting to note that the phase lead increases towards the bed, as expected for fixed-bed oscillatory boundary layer flow, but begins to decrease below the undisturbed bed level ($z = 0$). This suggests that the hydrodynamics in the lower sheet-flow layer are not being led from the stationary bed, but at some intermediate height close to the undisturbed bed level. Both models produce this reduction in phase lead. In the case of the UB model, this is because the flow is led by the fixed roughness at the undisturbed bed level. In the case of the UL model, it is likely to be related to the sudden increase in fluid–sediment velocity difference near the undisturbed bed level, as noted by Dong and Zhang (1999) and referred to earlier. A similar reduction in phase of the first harmonic near the base of the sheet-flow layer was found experimentally by Zara Flores and Sleath (1998) for sand with a median grain diameter of 0.41 mm and similar flow periods. Finally, as in Fig. 5, it may be noted that neither model is able to predict the magnitude of the offshore maximum in $\langle u \rangle$.

4.3. Sediment concentration

Comparisons between the computed and measured sediment concentrations are shown in Fig. 7 for the tests with $T = 7.5$ and 5 s (A7515 and A5010) and the three grain sizes (F, M and C). During the AOFT experiments, sediment concentrations were measured both within and above the sheet-flow layer (see

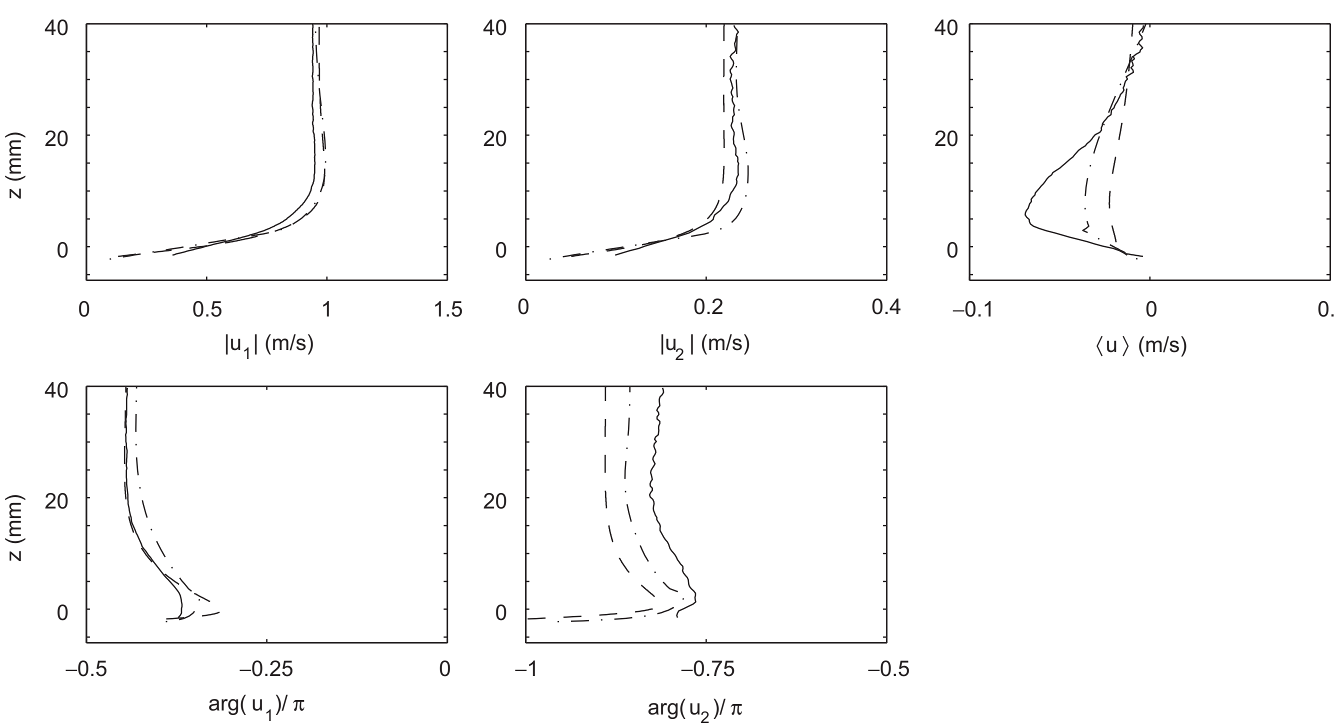

Fig. 6. Measured and predicted profiles of amplitude and phase of harmonics of velocity and mean velocity for LA406. Line type as in Fig. 5.

O'Donoghue and Wright, 2004a for details). For clarity, in this figure, comparisons are only made within the sheet-flow layer, where measurements were made using CCMs. For each case, four profiles are shown: three at phases 1, 3 and 7 (see Fig. 2), which correspond to flow reversal and maximum flow in the onshore and offshore directions, and one for the cycle mean. Note that the higher degree of scatter in the coarse sand concentration measurements compared to the other sands is due to the smaller ratio of CCM sensor spacing to grain diameter.

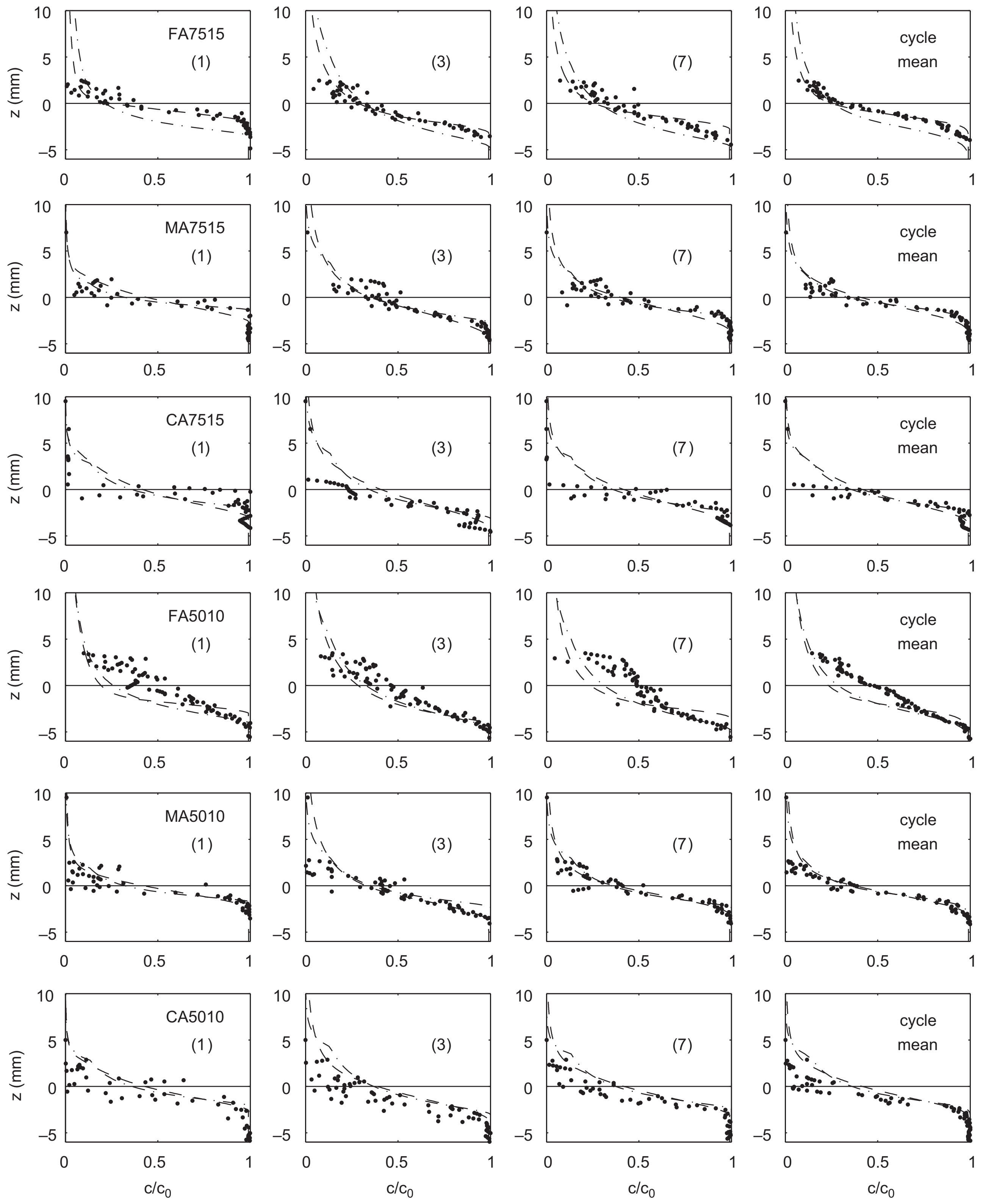

Fig. 7. Measured and predicted concentration profiles in the sheet-flow layer at phases 1, 3 and 7 (see Fig. 2) and time-averaged concentration profiles; two flows and three sands. Dots—measurement; dashed line—UL model; dashed–dotted line—UB model.

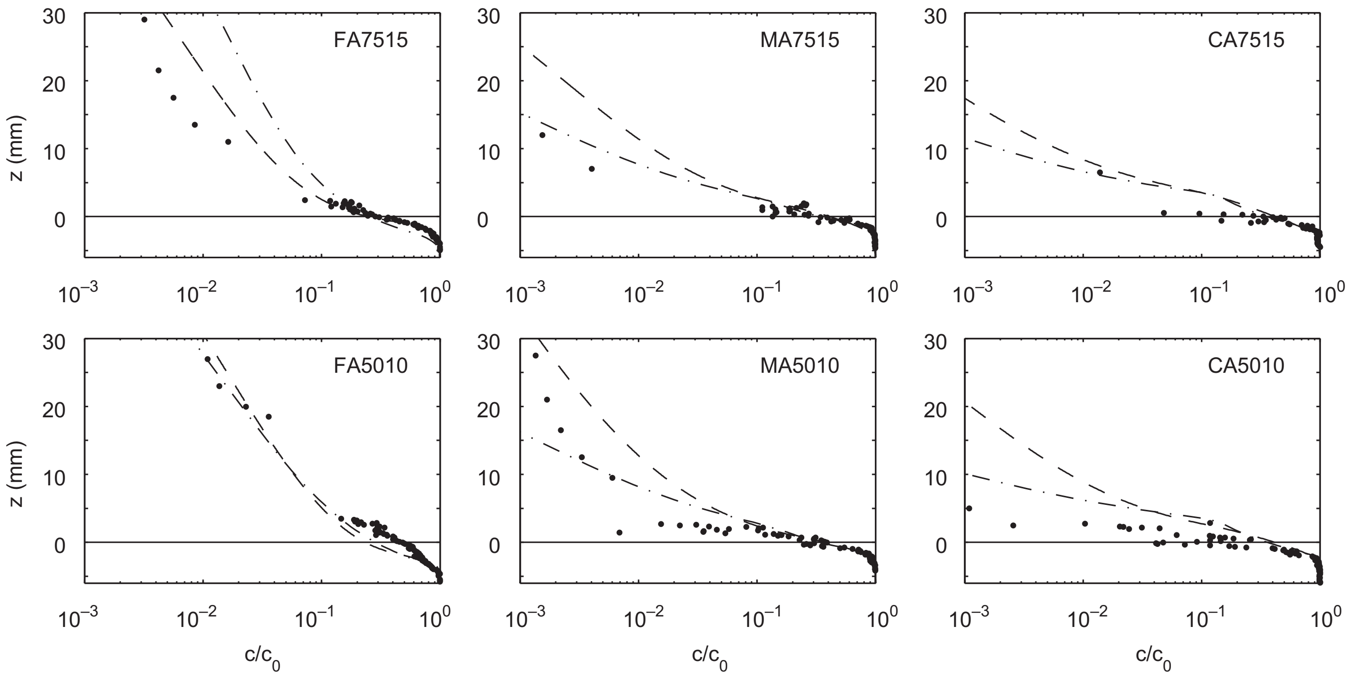

Fig. 8. Measured and predicted cycle-mean concentration profiles in the sheet-flow and suspension layers; two flows and three sands. Lines and symbols as in Fig. 7.

For the tests with $T = 7.5$ s, with the exception of the UB model for the FA7515 case, it is clear that there is very good overall agreement between the models and the data for all three sand sizes. This is particularly true in the lower part of the sheet-flow layer where $c/c_0 \rightarrow 1$, indicating that the erosion depth (where $c = c_0$) is being reasonably well predicted. In the case of the fine sand (FA7515), the UB model appears to be offset below the data by between 1 and 2 mm, the reason for which will become clear later. In the case of the coarse sand (CA7515), both models overpredict the concentration in the upper sheet-flow layer. In the UB model profiles for coarse sand, the top of the sheet-flow layer is visible as a change in slope [phase (3) at $z = 4$ mm].

For the tests with $T = 5$ s, the models agree reasonably well with the data for the medium and coarse sands as before. Again, the models tend to overpredict the concentrations in the upper sheet-flow layer in the coarse sand case, CA5010. However, for the fine sand (FA5010), the models appear to underpredict the concentrations quite substantially in the upper sheet-flow layer. This can also be seen clearly in the cycle-mean profile. In general, the results would appear to indicate that both the UL and UB models perform better for larger flow periods. For the UL model, this is may be due to the smaller acceleration generated by the larger flow period, which is partly reflected by the added mass (Li et al., 2008). However, the apparent discrepancy in the FA5010 case, and the less severe overprediction of concentration in the two coarse sand cases (CA5010 and CA7515), can also be explained by inconsistencies in the data, see Section 4.1, and this point will be returned to in the discussion section.

Fig. 8 shows a comparison of measured and predicted time-averaged concentration profiles extending into the suspension layer for the same six cases shown in Fig. 7. There are rather few measurements in the suspension layer, but the UB model generally shows better agreement with the cycle-mean concentration profiles for the medium and coarse sand cases, while the UL model shows better agreement in the fine sand cases. For the FA7515 case, in particular, the reason for the offset of the UB model results in the sheet-flow layer, discussed previously, becomes clear: the model is predicting too much sediment in suspension.

4.4. Erosion depth and sheet-flow layer thickness

The erosion depth and sheet-flow layer thickness are important quantities because they give a measure of how much sediment is in the water column and the overall scale of the sheet-flow layer, respectively. The sheet-flow layer thickness is estimated from the data by interpolating between the characterisation of the CCM measurements and the suction-sample/ABS measurements to find the height at which the concentration is 8% and then adding the erosion depth. The sheet-flow layer thicknesses are slightly different from those suggested by O'Donoghue and Wright (2004a) who used Eq. (1) alone to extrapolate a sheet-flow layer thickness.

Fig. 9 shows a comparison between the time variation in the erosion depth and sheet-flow layer thickness for the same six cases shown in Fig. 7. It is clear that for the erosion depth the models and the data are in reasonable agreement (mostly to within 1 mm of each other) except for the UB model in the FA7515 case discussed earlier. This agreement includes the correct phase behaviour, since the maxima and minima in the cycle from the models correspond to the data. The comparison between the models and the data for the sheet-flow layer thickness also shows reasonable agreement except for the two fine sand cases, where the UL model underpredicts for FA7515 and both models underpredict for FA5010 by up to 5 mm, and in the two coarse sand cases where the models overpredict for CA7515 and CA5010 by up to 2 mm. In the cases of FA5010, CA5010 and CA7515, the disagreement between measurement and models can be explained largely by the data inconsistency discussed in Section 4.1, which will be returned to in the discussion section. For FA7515, it is clear from Fig. 9 and Section 4.3 that the UB model predicts the sheet-flow layer thickness reasonably well but

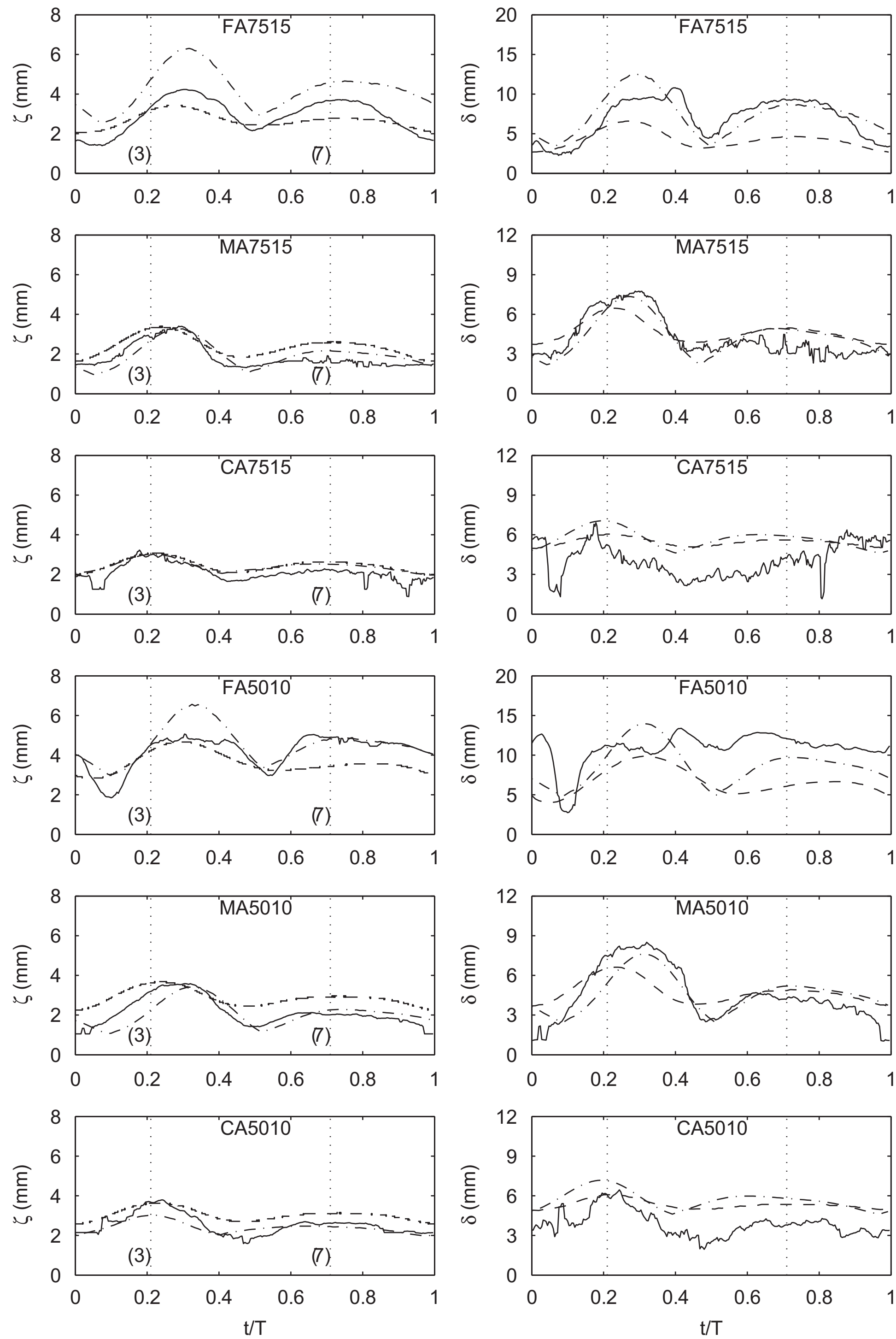

Fig. 9. Measured and predicted erosion depths (left side) and sheet-flow layer thicknesses (right side); two flows and three sands. Solid line—measurement; dashed line—UL model; dashed–dotted line—UB model; numbered dotted lines correspond to the phases in Fig. 2.

overpredicts the erosion depth because there is too much sediment in suspension.

The models predict the phases of the maxima and minima reasonably accurately for the sheet-flow layer thickness. It can be seen that the maxima and minima in both the sheet-flow layer thickness and the erosion depth correspond approximately to the onshore and offshore maxima and flow reversal in the free-stream velocity (as indicated by lines 3 and 7 representing the maxima in the flow). However, closer inspection of the phase behaviour reveals that there is an increasing phase lag for decreasing sand size. This is a manifestation of the so-called phase-lag effect discussed by Dohmen-Janssen et al. (2002), where finer sand in the sheet-flow layer responds more slowly than coarse sand to a given applied stress, and is the reason for the need to include the adjustment γ in the argument of θ in Eq. (4). In principle, there should also be a period effect for the phase lag (see Appendix B) whereby shorter flow periods produce larger phase lags but this can only be seen in the sheet-flow layer thickness data of MA7515 and MA5010. It is also interesting to point out the absence of strong asymmetry in the two flow half cycles, for both the measured erosion depths and

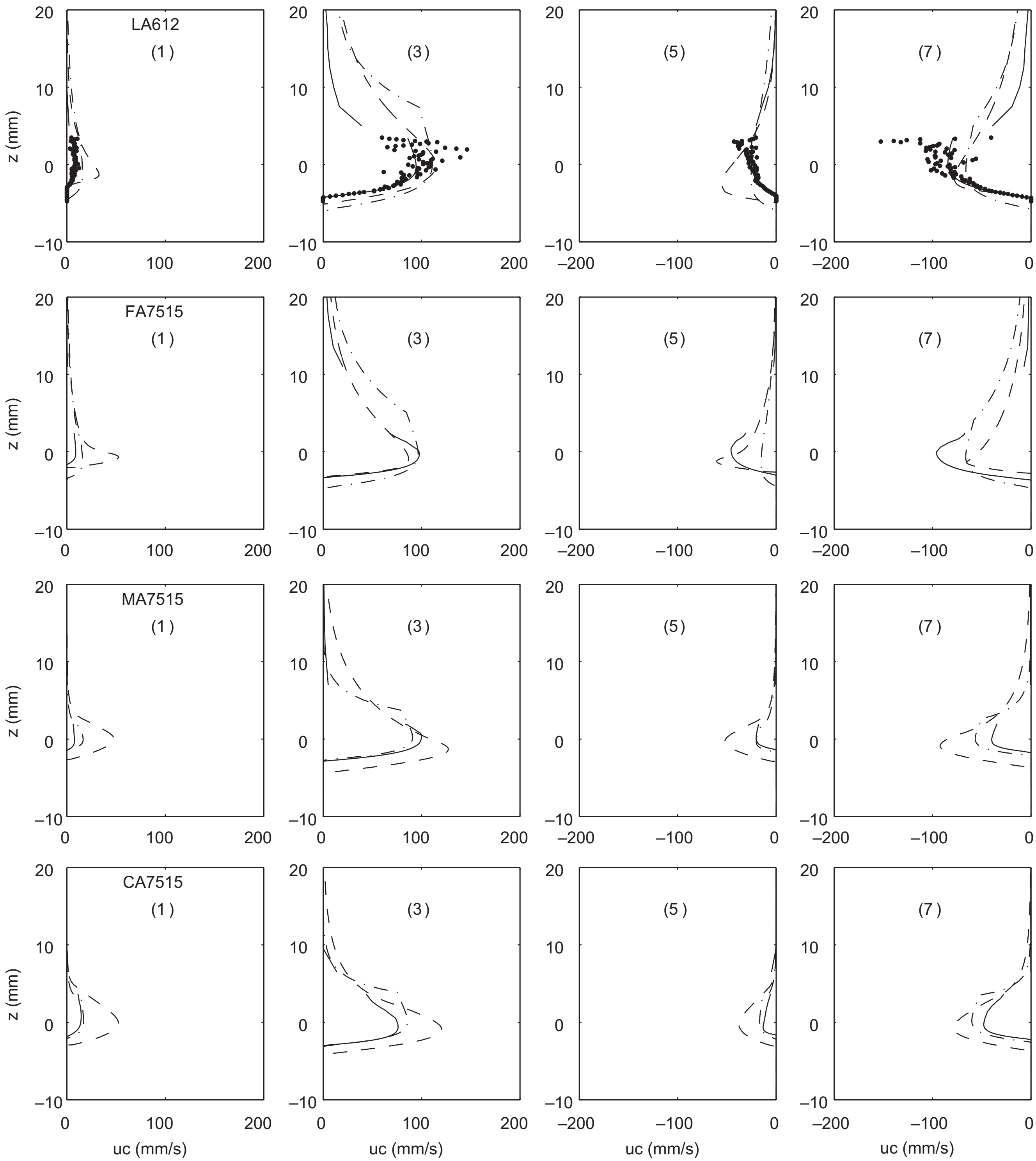

Fig. 10. Instantaneous sediment fluxes at phases 1, 3, 5 and 7 (Fig. 2) for LA612, FA7515, MA7515 and CA7515. Solid line—measurement with concentration based on Eq. (1); dots—measurement using actual CCM concentration measurements; dashed line—UL model; dashed–dotted line—UB model; break in solid line corresponds to gap between suction-sample/ABS and CCM data.

sheet-flow layer thicknesses, in the two fine sand cases compared with the medium and coarse sand cases. The two extra fine sand cases not included here (LA406 and LA612) also show a similar lack of asymmetry in their erosion depths (Fig. 4) and sheet-flow layer thicknesses (not shown). The models must produce some asymmetry as a result of different shear stresses in the flow half cycles (see for example Eq. (4)) but possibly, again as a result of the phase-lag effect, this asymmetry is not seen in the data for the fine sand cases. Thus, the models may not be representing the phase-lag effect fully. In contrast, in the medium sand cases, the models appear to underpredict the asymmetry in the sheet-flow layer thickness.

4.5. Sediment flux and transport rate

The sediment flux profiles were calculated from the computed and measured vertical profiles of velocity and sediment concentration shown previously. In the comparisons presented here the two LUBA experiments with fine sand (LA406 and LA612) are also included. As pointed out earlier, the CCM measurements become quite noisy towards the top of the sheet-flow layer, and have thus been replaced by their characterisations, see Eq. (1), to calculate the fluxes.

Figs. 10 and 11 show the sediment flux profiles at the four different phases (1, 3, 5 and 7 in Fig. 2) corresponding to flow reversal and maximum flow in the onshore and offshore directions, for LA612, FA7515, MA7515 and CA7515 (Fig. 10), and for LA406, FA5010, MA5010 and CA5010 (Fig. 11). To demonstrate the capability of the characterisation, fluxes determined directly from the CCM measurements, as well as from the Eq. (1) characterisation, are shown for the LA612 case in Fig. 10. It is clear that the flux profiles based on the CCM characterisation capture the behaviour of the flux profiles very well.

Generally, the predicted instantaneous model fluxes agree well with the measured fluxes, both in terms of the magnitude and elevation of the maximum flux. The UL model tends to predict the flux better at maximum flow [phases (3) and (7)] and the UB

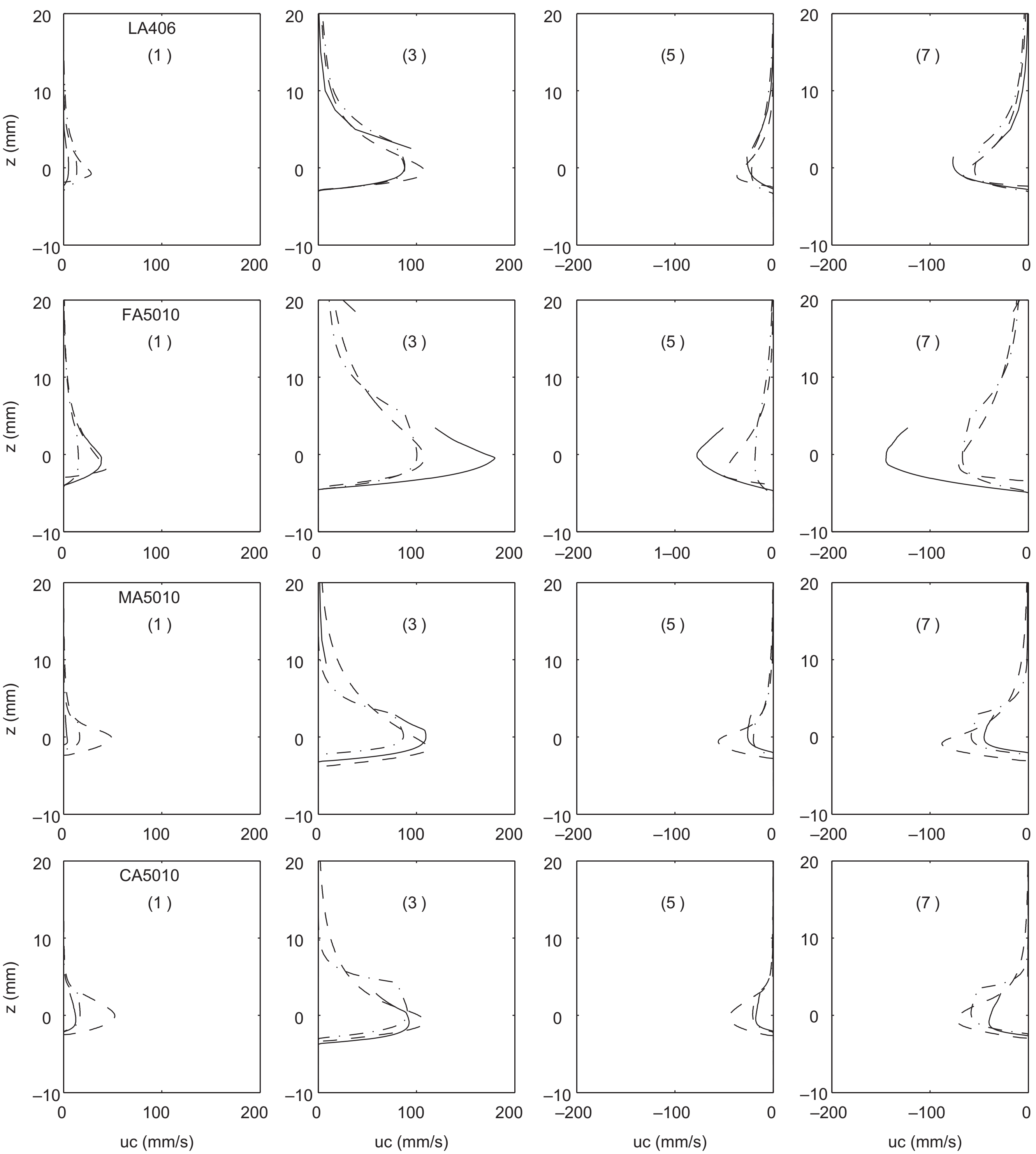

Fig. 11. Instantaneous sediment fluxes at phases 1, 3, 5 and 7 (Fig. 2) for LA406, FA5010, MA5010 and CA5010 (symbols are the same as in Fig. 10).

model tends to predict the flux better at flow reversal [phases (1) and (5)]. However, both models fail to predict the magnitude of the near-bed maximum in the FA5010 case. Over all three grain sizes, the models appear to be able to predict the fluxes in tests with $T = 7.5$ s better than with $T = 5$ s. It is clear from the profiles that with the exception of the fine sand cases, see Section 4.4, the onshore fluxes occur at lower levels than the offshore fluxes due to the larger erosion depths associated with larger shear stresses of the onshore flow. Notice that for FA5010, in particular, there is a large gap between the CCM and suction-sample measurements (the break in the solid line), whereas in the other cases the gap between the CCM and suction-sample/ABS measurements is much smaller. This point will be returned to in the next section.

Fig. 12 shows profiles of the current-related flux, $\langle u\rangle\langle c\rangle$, and true cycle-mean flux, $\langle uc\rangle$, for each of the eight cases being considered. In the fine sand cases the current-related and the cycle-mean flux are offshore dominated; in the medium and coarse sand cases the fluxes are onshore dominated. The current-

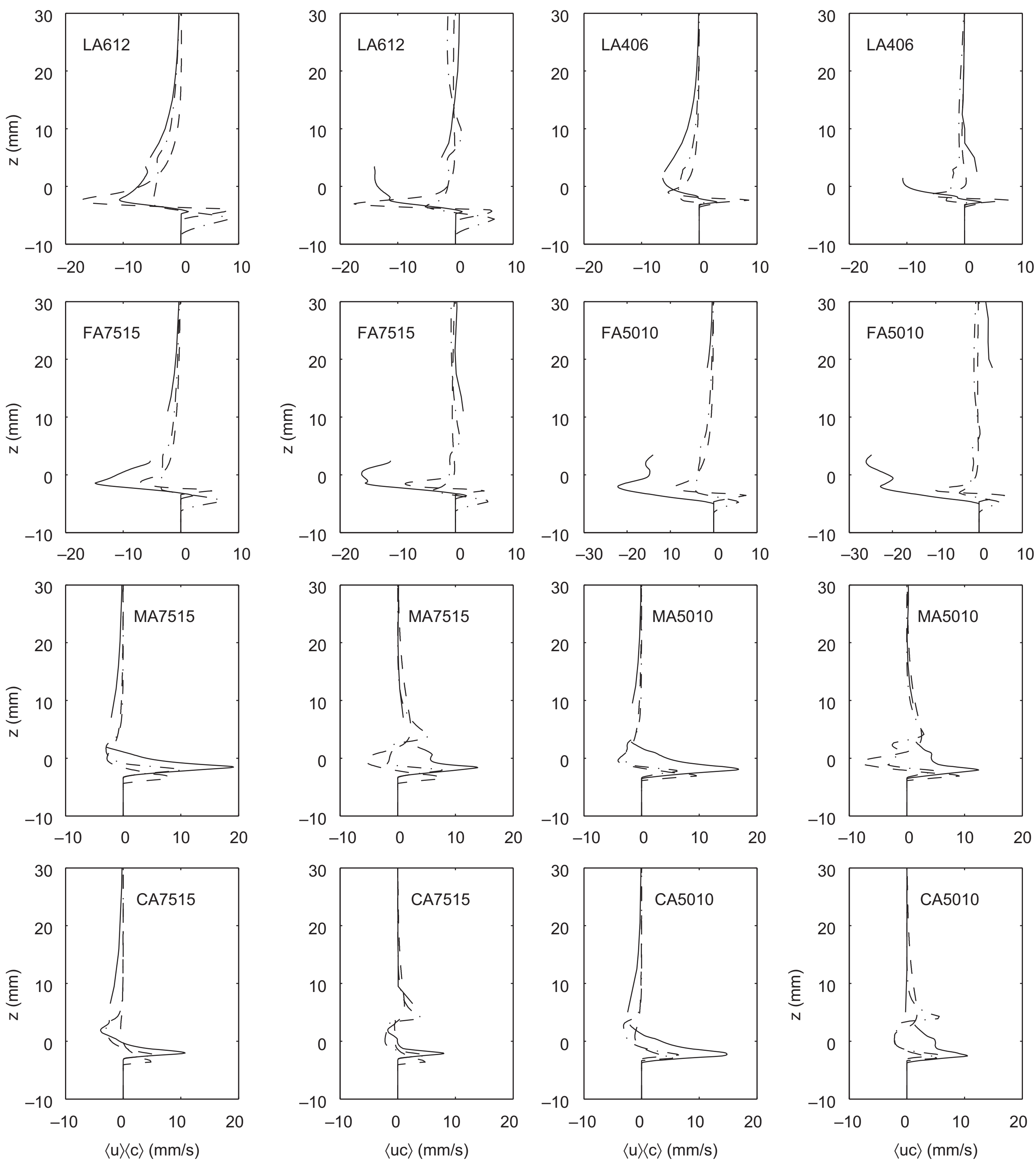

Fig. 12. Measured and predicted profiles of current-related flux, $\langle u\rangle\langle c\rangle$, and true cycle-mean flux, $\langle uc\rangle$, for all eight cases (symbols as in Fig. 10).

related flux profiles predicted by the models have very similar vertical structure to those of the data with a single onshore maximum close to the stationary bed and offshore maximum higher up in the sheet-flow layer (which are clearly linked to the onshore and offshore maxima discussed in Section 4.2). In the fine sand cases, the UL model predicts the position of the offshore maximum well in all of the cases and the position of the onshore maximum in all but the FA5010 case. The UB model predicts the positions of the offshore and onshore maxima well in the LA406 and FA5010 cases; the poorer prediction in the other cases is related to the poorer prediction of the erosion depth. For the medium and coarse sand cases, the position of the onshore maximum is reasonably predicted by both models but the position of the offshore maximum is less well predicted. For the fine sand cases, the models overpredict the magnitude of the onshore maximum but, more significantly, tend to underpredict the magnitude of the offshore maximum. For the medium and coarse sand cases, the models underpredict quite substantially the magnitude of the onshore maximum and predict reasonably well the magnitude of the offshore maximum. Above the sheet-flow layer, the models predict the flux profiles measured by the suction-sample/ABS measurements reasonably well.

It can be seen from the true cycle-mean flux profiles $\langle uc \rangle$ that the models in general produce magnitudes which are approximately equivalent to the data and that these are an order of magnitude less than the instantaneous fluxes (see Figs. 10 and 11). The flux profiles based on the suction-sample/ABS data are again reasonably well reproduced. The comparisons of the onshore and offshore maxima follow those of the current-related flux. In fact, with the exception of the upper part of the sheet-flow layer, the differences between measured and predicted cycle-mean flux profiles occur mainly as a result of differences in the current-related flux. In the medium and coarse sand cases, the most significant difference is the underprediction of the magnitude of the onshore maximum. This in turn is probably due to the models' failure to predict the magnitude of the onshore cycle-mean velocity maximum (see Section 4.2) because of a lack of asymmetry in the predicted erosion depth and differences in the velocity near the erosion depth. For the fine sand cases, the underprediction of the offshore maximum in the current-related flux is the more significant difference. This is related to the models' underprediction of the offshore maximum in the cycle-mean velocity which results from turbulence asymmetry in the two flow half cycles. Towards the top of the sheet-flow layer in the fine sand cases, there is an increasingly important difference which is wave-related ($\langle uc \rangle - \langle u \rangle \langle c \rangle$) but it should be remembered that this region is where the CCM measurements are most noisy.

4.6. Net sediment transport rate

The net transport rate can in principle be determined from the measured vertically integrated, cycle-mean flux profiles

$$\langle q_i \rangle = \int_{-z_1}^{h} \langle uc \rangle \, dz, \tag{8}$$

where $-z_1$ is always below the instantaneous erosion depth. However, there are also the completely independent measurements of the net transport rate based on mass conservation and the sand collected at the ends of the test section, referred to here as $\langle q_m \rangle$. O'Donoghue and Wright (2004b) used this value of $\langle q_m \rangle$ to determine what the missing flux had to be in the gap between the characterised CCM and suction-sample measurements such that the net vertically integrated, cycle-mean flux and $\langle q_m \rangle$ were equal to one another. However, in all the cases other than FA5010, where the gap is too large (see Fig. 12), it is reasonable to linearly interpolate between the CCM and suction-sample/ABS measurements and obtain a second estimate by integrating the cycle-mean flux, $\langle q_i \rangle$ in Eq. (8). Thus, in all but one case it is possible to have two independent measurements of net transport rate, $\langle q_m \rangle$ and $\langle q_i \rangle$, such that a best estimate, $\langle q \rangle$, and error, $\Delta\langle q \rangle$, (based on $\langle q \rangle = (\langle q_m \rangle + \langle q_i \rangle)/2$ and $\Delta\langle q \rangle = |\langle q_m \rangle - \langle q_i \rangle|/2$) can be derived. The values $\langle q_m \rangle$ and $\langle q_i \rangle$ are given in Table 2. It can be seen that there is reasonable agreement between the values of $\langle q_m \rangle$ and $\langle q_i \rangle$ and that the net transport rate is onshore (positive) for the medium and coarse sands and offshore for the fine sand cases.

Table 2
Measured net sand transport rates for the experiments listed in Table 1.

Test	D (mm)	$\langle q_m \rangle$ (mm^2/s)	$\langle q_i \rangle$ (mm^2/s)
FA5010	0.13	−128	–
FA7515	0.13	−88	−99
MA5010	0.27	53	56
MA7515	0.27	36	54
CA5010	0.46	44	32
CA7515	0.46	34	13
LA406	0.13	−8	−26
LA612	0.13	−61	−76

$\langle q_m \rangle$ is net sand transport rate based on mass conservation method and $\langle q_i \rangle$ is based on integration of the flux profile.

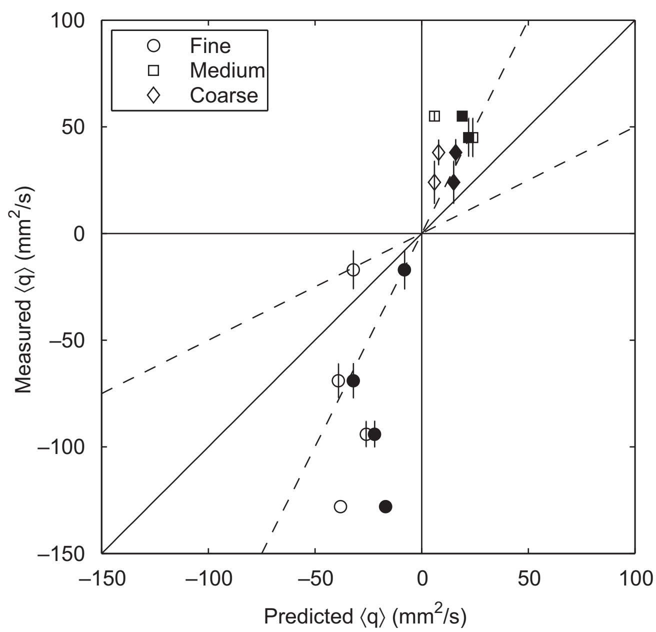

Fig. 13. Measured versus predicted net sand transport rates for the eight AOFT cases. Solid symbols—UL model; open symbols—UB model; solid line—perfect agreement; dashed line—factor of two difference.

A comparison of the measured net transport rates and associated errors from Table 2 and the predicted values from the models is shown in Fig. 13. The results show that both models predict the correct direction of net transport in all eight cases: offshore for the fine sand cases and onshore for the medium and coarse sands. The UL model predicts the magnitude of the net transport better for the medium and coarse sands and the UB model predicts the magnitude better for the fine sand. Overall, the UL model is better able to predict the magnitude of the net transport rate with a total of five out of eight cases within a factor of two of the data as compared to three out of eight for the UB model. For predicting to within a factor of four this improves to seven out of eight for both models. Except for one fine-grained case (LA406 with the UB model), the models produce magnitudes that are smaller than those measured. Referring back to Sections 4.4 and 4.5, it seems likely that this underprediction relates to the differences in the velocity profiles and the amounts of asymmetry in the sheet-flow layer thickness and erosion depth between the model and experimental results. This asymmetry allows the flow to dig deeper under the crest, thus producing onshore net transport. In the fine sand cases, less asymmetry than predicted, combined with a larger offshore cycle-mean velocity, leads to stronger offshore net transport and more asymmetry than predicted in the medium and coarse sand cases leads to stronger onshore net transport. This explanation is consistent with the results of Liu and Sato (2006) who compared their two-phase flow model with the starred experiments in Table 1. They were able to produce closer net transport rate agreement than the present study by using the values of U_1 and U_2/U_1 derived from the tunnel's piston movement, rather than those based on the UVP measurements quoted in Table 1, and also by forcing their modelled velocity to go to zero at the same elevation as the data (the erosion depth).

5. Discussion

This intercomparison has demonstrated the importance of achieving consistency in the data as a basis for the critical testing of models. The question of consistency arose in three out of the eight cases tested (FA5010, CA5010 and CA7515). In these cases, the instantaneous integrated measured sediment concentration in the water column did not correspond to the instantaneous erosion depth. In particular, in one fine sand case (FA5010) there appeared to be too much sediment in the water column for the measured erosion depth and in two coarse sand cases (CA5010, CA7515) there appeared to be too little sediment in the water column for the measured erosion depth.

It is worthwhile considering the possible reasons for this inconsistency. One possibility is that it relates to the uncertainty in the measurement of smaller concentrations higher up in the flow. This is certainly true of the CCM measurements and may also be true of the suction-sample measurements. However, this does not explain why the measurements would be consistently higher for fine sands and lower for coarse sands. The other possibility is that of horizontal non-uniformity or some end effect in the AOFT. For example, upstream of the measuring point there may have been more (or less in the case of the coarse sand) sediment in the water column such that when it was advected past the measuring point it gave an anomalously high (or low) concentration reading. While this might seem unlikely, it should be realised that at any given phase, sediment can originate from anywhere along a length of the tunnel corresponding to a 'reach' of d_0 which includes the measuring point (where d_0 is the orbital diameter given approximately by $2[U_1^2+U_2^2]^{0.5}/\omega$) and it can come from as far away as d_0 from the measuring point. Thus, in the cases considered here, conditions must be horizontally uniform typically for ± 2 to 3 m on either side of the measuring point to rule out horizontal non-uniformity. This is quite a stringent constraint when one considers that the inconsistency in the position of the erosion depth being discussed is at most a few mm and that flow disturbance due to the presence of the suction samplers, for example, can cause quite strong local variations in the bed level (see O'Donoghue and Wright, 2004b) and presumably can effect the sediment in suspension.

It is also important to demonstrate improved agreement between the models and the data when consistency is restored, whatever the reason for the inconsistency. Here, the most striking example, FA5010, is considered. Ideally, one would like to be able to remove the apparent extra amount of sediment by some adjustment to the concentration measurements such that consistency is restored. A possible method for making an adjustment to the concentration measurements, which is discussed in Appendix B for symmetric flow cases, is used here for FA5010. In this case, the adjustment will reduce the concentration but the approach can equally be applied to the coarse sand cases where the adjustment would increase the concentrations. It should be pointed out that this is not the only way to restore consistency but is used here to demonstrate the principle.

Fig. 14 shows a comparison between the model predictions and the adjusted cycle-mean concentration profile and time-series of sheet-flow layer thickness for FA5010. It can be seen that with consistency restored in the data, the model results and the data are in much closer agreement in the upper sheet-flow layer for the mean concentration. Also, there is closer agreement in the sheet-flow layer thickness, but there are still differences between the models and the data. Though not shown here, restoring consistency in the two coarse-grained cases improves the comparison as well. If it is assumed that the inconsistency arises from there being too much sediment in the water column, rather than a systematic concentration measurement error, then reducing the concentration measurements will also reduce the net transport rate. This may mean that $\langle q_m \rangle$ determined from mass conservation can no longer be related to the local vertically integrated, cycle-mean flux profile. While this is difficult to test for the FA5010 case, because of the CCM/suction-sample gap, it is likely that this would lead to an improvement in the net transport comparison shown in Fig. 13.

Both models predict profiles of velocity, concentration and flux reasonably well and are able to predict the correct net transport rate directions consistently. However, they tend to underpredict the magnitude of the net transport rate. This underprediction was associated with both models' inability to predict the correct amount of asymmetry in the sheet-flow layer thickness and

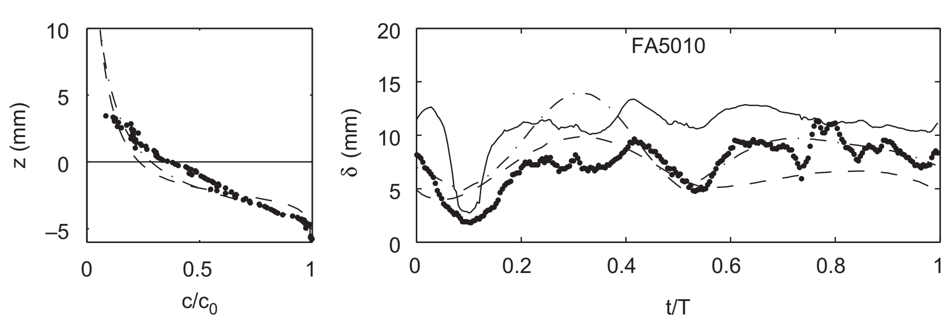

Fig. 14. Measured and predicted cycle-mean concentration profile and time-varying sheet-flow layer thickness for FA5010. Solid line—unadjusted sheet-flow layer thickness data; dots—adjusted data; dashed line—UL model; dashed–dotted line—UB model.

erosion depth, together with differences in the velocity between model and data, see Section 4.6. It should be pointed out, however, that agreement with the observed net transport rate is quite a challenge for the models because of the difference in magnitude between the net and maximum instantaneous transport rates.

6. Conclusions

Two numerical models for oscillatory sheet-flow conditions, one of which is based on the two-phase approach and the other is based on a two-layer approach, are described in this paper. Both models are applied to a series of experimental conditions from a flow tunnel, under near field-scale conditions, where detailed measurements of velocity, sediment concentration and net sediment transport rate were taken. The results from the models are compared with the experimental data from eight asymmetric (velocity-skewed) oscillatory flow cases with three different grain sizes ranging from 0.13 to 0.46 mm. Despite using very different approaches, the two-phase model and the two-layer model are capable of reproducing reasonably well the profiles of velocity, sediment concentration and flux as well as the erosion depth and sheet-flow layer thickness. The model results also reflected the increasing importance of phase-lag effects seen in the data as the sand becomes finer. The models yielded net sediment transport rates that were in the same direction as the measured net transport rates: offshore for the fine sand cases and onshore for the medium and coarse sands. In terms of the magnitude of the net transport rate, agreement to within a factor of two was achieved in five out of eight cases for the two-phase model and in three out of eight cases for the two-layer model.

Acknowledgements

This work was funded by the UK Engineering and Physical Sciences Research Council (EPSRC) partly under the 'LUBA' project, GR/R23596, GR/R23589 and GR/R23572, and partly under the 'SANTOSS' project, GR/T28089 and also by the UK Natural Environment Research Council (NERC) under the 'FORMOST' project, NE/E015123/1.

Appendix A. Changes made in the updated UB model

In the sheet-flow layer, the updated UB model uses a prescribed concentration profile with the same functional form as Eq. (1) given by

$$c(z,t) = \frac{c_0}{1 + [(c_0/c_\delta) - 1][(z+\zeta(t))/\delta(t)]^{1.5}}, \tag{A.1}$$

as opposed to the quadratic function that was used in the original model. In Eq. (A.1), $\zeta(t)$ is the erosion depth determined in the model at each time step and $\delta(t)$ the sheet-flow layer thickness given by

$$\frac{\delta(t)}{D} = \delta_{\min} + \delta_\theta \theta(\omega t - \gamma), \tag{A.2}$$

where $\delta_{\min}$, δ_θ and γ are parameterised in Appendix B.

In the suspension layer, the updated UB model uses a fixed equivalent roughness given by

$$\frac{k_s}{D} = \begin{cases} 2, & \langle\theta\rangle \leqslant 1, \\ 2 + 3.7(\langle\theta\rangle - 1), & \langle\theta\rangle > 1, \end{cases} \tag{A.3}$$

where $\langle\theta\rangle$ is the cycle-mean Shields parameter given by the outer-flow solution. Eq. (A.3) is the same as the roughness used in the model of Malarkey et al. (2003) except that here it uses the cycle-mean rather than the instantaneous Shields parameter. Also, the origin of the roughness length scale, z_0 ($=k_s/30$) is fixed at the undisturbed bed level ($z=0$) rather than being allowed to vary as in the original model. Both of these modifications help to simplify the numerical aspects of the model, see Malarkey et al. (2003). However, the use of Eq. (A.3), when $\langle\theta\rangle > 1$, requires that the model be run a number of times to determine iteratively a k_s value that is consistent with the cycle-mean Shields parameter.

Appendix B. Parameterising $\delta_{\min}$, δ_θ and γ in Eq. (4) for the UB model

B.1. Introduction

Malarkey et al. (2003) assumed that $\delta_{\min}=10$, $\delta_\theta=6$ and that the sheet-flow layer responded quasi-steadily to the shear stress ($\gamma=0$) based on a comparison with the experiments of Horikawa et al. (1982). This was found to produce reasonable results for medium and coarse sands but poor results for fine sands in comparison with the data of Dohmen-Janssen et al. (2001). The poor results for the fine sand were attributed partly to the assumption of quasi-steadiness and partly to the formula substantially under-predicting the sheet-flow layer thickness. This appendix explains how the coefficients for the prescription of the sheet-flow layer thickness in Eq. (4), $\delta_{\min}$, δ_θ and γ, for the UB model have been parameterised. The parameterisations are based on AOFT experiments involving symmetric flow (O'Donoghue and Wright, 2004a; Wright and O'Donoghue, 2002; Li et al., 2003), as listed in Table B1, where A_1 is the orbital amplitude ($=U_1/\omega$). While this appendix is necessarily related to the UB model, the process of parameterisation provides some useful insights into the behaviour of the sheet-flow layer thickness for different flow conditions.

B.2. Method

The measured time-varying concentration $c_m(z,t)$, using both CCM and suction-sample or ABS measurements is first adjusted by some quantity $P(t)$ such that the adjusted concentration $c(z,t)$ satisfies conservation of sediment volume (based on the position of the erosion depth)

$$\zeta(t)c_0 = \int_{-\zeta}^{h} c(z,t)\,dz, \tag{B.1}$$

where $c(z,t) = \{1 - P(t)F(z)\}c_m(z,t)$ and $F(z) = (z+\zeta)/\delta$ when $(z+\zeta)/\delta \leqslant 1$ and 1 when $(z+\zeta)/\delta > 1$. The reason for an adjustment with this functional form is that the concentration measurements become increasingly uncertain further away from the stationary bed level at $z=-\zeta(t)$. The conservation requirement expressed in Eq. (B.1) is applied within certain tolerance limits based on the

Table B1
AOFT symmetric flow experiments, results from which are used to parameterise sheet-flow layer thickness in the UB model. U_1 and A_1 ($=U_1/\omega$) is based on the uppermost UVP measurement when available.

Test	D (mm)	T (s)	U_1 (m/s)	A_1 (m)
F512[a]	0.13	5	1.43	1.14
F7515[a]	0.13	7.5	1.18	1.41
M512[a]	0.27	5	1.43	1.14
M7515[a]	0.27	7.5	1.18	1.41
LS612	0.13	6	1.20	1.15
LS915	0.13	9	1.00	1.44

[a] Corresponds to tests undertaken by O'Donoghue and Wright (2004a, b).

value of c_0 measured below the erosion depth, see Section 4.1. Once the adjusted concentration (c) is found, a new sheet-flow layer thickness δ, which satisfies Eq. (A.1) is determined using the same least-squares fitting technique described by O'Donoghue and Wright (2004a). The sheet-flow layer thickness is forced to be symmetric in the two flow half cycles, $\delta_s(t) = \{\delta(t)+\delta(t+T/2)\}/2$, and is then fitted to the following equation:

$$\delta_s(t) - \min(\delta_s) = D\delta_\theta \theta(\omega t - \gamma), \tag{B.2}$$

where θ is time-varying Shields parameter from the outer-flow solution of the model, with a roughness k_s given by Eq. (A.3), adjusted by some optimum phase lag γ. Thus, in Eq. (4) $\delta_{\min} = \min(\delta_s)/D$.

B.3. Results

There are four fine sand cases and two medium sand cases in Table B1. An example of the fit to Eq. (B.2) for one of the fine sand cases (F512) is shown in Fig. B1. It is clear that in the symmetric flow case, this approximation provides a reasonable description of the sheet-flow layer thickness, though it fails to represent the higher frequency variation.

The results for $\delta_{\min}$, γ and δ_θ for fine sand are shown in Fig. B2. It can be seen that while both $\delta_{\min}$ and γ decrease with increasing oscillatory flow period, δ_θ increases with period. This period behaviour can be understood in terms of the response time of the sediment to the time-varying stress, or what Dohmen-Janssen et al. (2002) referred to as the phase-lag effect. As the period decreases, the response of the sheet-flow layer thickness becomes increasing delayed (γ increases) and increasingly decoupled from the time-varying part of the stress (δ_θ decreases). However, since the minimum sheet-flow layer thickness must be related to the mean shear stress, $\langle\theta\rangle$, in the same way as it is in steady flow, and this will increase with decreasing period, so $\delta_{\min}$ must increase. Thus, it is reasonable to expect that as $T\to 0$, $\delta_{\min}/\langle\theta\rangle$ will reach a maximum and $\delta_\theta \to 0$.

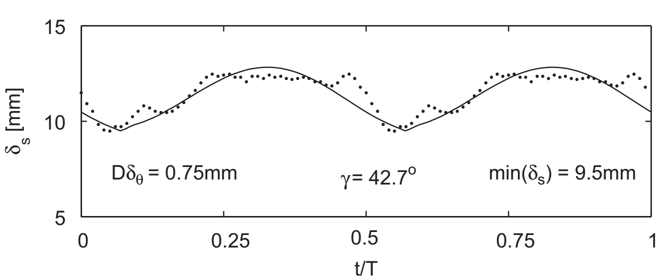

Fig. B1. Fit of Eq. (B.2) to δ_s for case F512.

It can be seen in Fig. B2 that neither $\delta_{\min}/\langle\theta\rangle$ nor γ show any significant orbital amplitude dependence and are well described by a linear fit to the period. However, δ_θ shows both period and orbital amplitude dependence. The simplest representation of the δ_θ behaviour is to assume that it depends linearly on the period, as depicted in Fig. B2, with a slope and intercept that depend on the orbital amplitude. This simple representation implies that there is a minimum flow period, for a given orbital amplitude, below which $\delta_\theta = 0$. This is probably unrealistic since $\theta_{\max}$ increases with decreasing period, and so it is likely that δ_θ approaches zero more gradually. Thus, while the linear relationship is reasonable for present purposes it is more plausible that for small δ_θ the relationship is not linear but of the form $\delta_\theta = K(A_1)T^n$. In the present linear parameterisation, the dependence of the slope and intercept on the orbital amplitude was found to be a quadratic and linear, respectively, such that $\delta_\theta \to 0$ as $A_1 \to 0$. The resulting formulae for $\delta_{\min}$, γ and δ_θ, obtained by least-squares fitting, which are shown in Fig. B2, are given by

$$\delta_{\min} = (45 - P_1 T)\langle\theta\rangle, \tag{B.3a}$$

$$\gamma = 61 - P_2 T, \tag{B.3b}$$

$$\delta_\theta = (P_3 A_1 - P_4 A_1^2)T - P_5 A_1 - P_6, \tag{B.3c}$$

where γ is in degrees, $P_1 = 3.3\,\mathrm{s}^{-1}$, $P_2 = 3.5\,\mathrm{s}^{-1}$, $P_3 = 42.89\,\mathrm{m}^{-1}\,\mathrm{s}^{-1}$, $P_4 = 22.22\,\mathrm{m}^{-2}\,\mathrm{s}^{-1}$, $P_5 = 58.17\,\mathrm{m}^{-1}$, $P_6 = 26.63$, A_1 in meters, T in seconds and defined by the following region of applicability $(P_5A_1 - P_6)/(P_3A_1 - P_4A_1^2) < T < 52/P_1$. For a given orbital amplitude, as the flow period increases, the maximum Shields parameter decreases until sheet-flow conditions no longer apply. For example, if the sheet-flow limit is taken to be $\theta_{\max} = 1$, then when $A_1 = 1.5$ m this upper limit corresponds to $T = 11.7$ s. Also, it can be seen from Eq. (B.3a) that $\delta_{\min}$ will be equal to its steady flow equivalent ($\delta_{\min} = 10\langle\theta\rangle$) c.f. Wilson (1989) when $T = 10.6$ s. However, it is important to point out that these formulae should not be applied to conditions too far away from those listed in Table B1.

In the medium sand case, for the tests with $T = 5$ and 7.5 s, respectively, $\delta_{\min} = 14$ and 8, $\gamma = 44^\circ$ and 28° and $\delta_\theta = 18$ and 9. The variations in $\delta_{\min}$ and γ are similar to the fine sand equivalents and can be described by the linear equations $\delta_{\min} = \langle\theta\rangle(19–0.83T)$ and $\gamma = 75–6.2T$, respectively. Now, while δ_θ should also behave qualitatively in the same way as the fine sand case, the lack of cases in this instance meant that a representative δ_θ based on the mean of the two values (13.5) had to be used. Since there are no symmetric flow cases for coarse

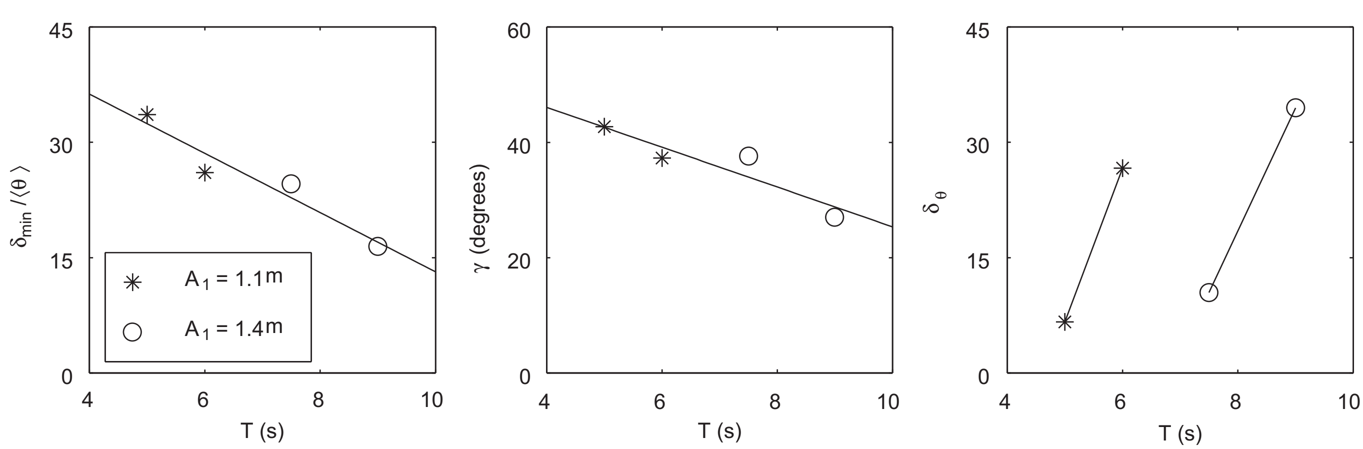

Fig. B2. Dependence of $\delta_{\min}$, γ and δ_θ on wave period and amplitude for $D = 0.13$ mm.

sand the existing parameterisation namely $\delta_{\min}=10$, $\delta_\theta=6$ and $\gamma=0$ has been used. Summarising, over the three grain sizes the parameterisation in non-dimensional form is as follows:

$$\delta_{\min}=\begin{cases}(45-0.0084T_*)\langle\theta\rangle, & D=0.13\,\text{mm}\\(17-0.0018T_*)\langle\theta\rangle, & D=0.27\,\text{mm}\\10, & D=0.46\,\text{mm}\end{cases},\tag{B.4a}$$

$$\delta_\theta=\begin{cases}(P_{1*}A_*-P_{2*}A_*^2)T_*-P_{3*}A_*-P_{4*}, & D=0.13\,\text{mm}\\13.5, & D=0.27\,\text{mm}\\6, & D=0.46\,\text{mm}\end{cases},\tag{B.4b}$$

$$\gamma=\begin{cases}59-0.0075T_*, & D=0.13\,\text{mm}\\75-0.0135T_*, & D=0.27\,\text{mm}\\0, & D=0.46\,\text{mm}\end{cases},\tag{B.4c}$$

where $P_{1^*}=3.93\times10^{-6}$, $P_{2^*}=1.06\times10^{-10}$, $P_{3^*}=2.27\times10^{-3}$, $P_{4^*}=22.2$, $T_*=T(g^2/\nu)^{1/3}$, $A_*=A_1(g/\nu^2)^{1/3}$ and ν is the kinematic viscosity ($=1\,\text{mm}^2/\text{s}$).

References

Ahilan, R.V., Sleath, J.F.A., 1987. Sediment transport in oscillatory flow over flat beds. Journal of Hydraulic Engineering 113 (3), 308–322.

Amoudry, L., Hsu, T.J., Liu, P.L.F., 2008. Two-phase model for sand transport in sheet flow regime. Journal of Geophysical Research 113, C03011.

Asano, T., 1990. Two-phase flow model on oscillatory sheet-flow. In: Proceedings of the 22nd International Conference on Coastal Engineering. Delft, the Netherlands, pp. 2372–2384.

Calantoni, J., Holland, K.T., Drake, T.G., 2004. Modelling sheet-flow sediment transport in wave-bottom boundary layers using discrete-element modelling. Philosophical Transactions of the Royal Society of London, Series A 362, 1987–2001.

Davies, A.G., Li, Z., 1997. Modelling sediment transport beneath regular symmetrical and asymmetrical waves above a plane bed. Continental Shelf Research 17 (5), 555–582.

Davies, A.G., Ribberink, J.S., Temperville, A., Zyserman, J.A., 1997. Comparisons between sediment transport models and observations made in wave and current flows above plane beds. Coastal Engineering 31 (1–4), 163–198.

de Leeuw, C.J., 2005. Model predictions of wave-induced sediment transport on the shoreface. M.Sc. Thesis, University of Twente, Enschede, The Netherlands, 115 pp.

Dohmen-Janssen, C.M., 1999. Grain size influence on sediment transport in oscillatory sheet flow: phase lags and mobile-bed effects. Ph.D. Thesis, Delft University of Technology, Delft, The Netherlands, 246 pp.

Dohmen-Janssen, C.M., Hanes, D.M., 2002. Sheet flow dynamics under monochromatic nonbreaking waves. Journal of Geophysical Research 107 (C10), 3149.

Dohmen-Janssen, C.M., Hassan, W.N., Ribberink, J.S., 2001. Mobile-bed effects in oscillatory sheet flow. Journal of Geophysical Research 106 (C11), 27103–27115.

Dohmen-Janssen, C.M., Kroekenstoel, D.F., Hassan, W.N., Ribberink, J.S., 2002. Phase lags in oscillatory sheet flow: experiments and bed load modelling. Coastal Engineering 46 (1), 61–87.

Dong, P., Zhang, K., 1999. Two-phase flow modelling of sediment motions in oscillatory sheet flow. Coastal Engineering 36 (2), 87–109.

Dong, P., Zhang, K., 2002. Intense near-bed sediment motions in waves and currents. Coastal Engineering 45 (2), 75–87.

Guizien, K., Dohmen-Janssen, C.M., Vittori, G., 2003. 1DV bottom boundary layer modeling under combined wave and current: Turbulent separation and phase lag effects. Journal of Geophysical Research 108 (C1), 3016.

Horikawa, K., Watanabe, A., Katori, S., 1982. Sediment transport under sheet flow conditions. In: Proceedings of the 18th International Conference on Coastal Engineering. Cape Town, South Africa, pp. 1335–1352.

Hsu, T.J., Jenkins, J.T., Liu, P.L.F., 2003. On two-phase sediment transport: Dilute flow. Journal of Geophysical Research 108 (C3), 3057.

Janssen, M., Hassan, W., van der Wal, R., Ribberink, J., 1997. Grain-size influence on sand transport mechanisms. In: Proceedings of third International Conference on Coastal Dynamics. Plymouth, pp. 58–67.

Justesen, P., 1991. A note on turbulence calculations in the wave boundary layer. Journal of Hydraulic Research 29 (5), 699–711.

Kaczmarek, L.M., Ostrowski, R., 2002. Modelling intensive near-bed sand transport under wave-current flow versus laboratory and field data. Coastal Engineering 45 (1), 1–18.

Li, L., Sawamoto, M., 1995. Multi-phase model on sediment transport in sheet-flow regime under oscillatory flow. Coastal Engineering in Japan 38 (2), 157–178.

Li, M., Pan, S., O'Connor, B.A., 2003. Acoustic back scattering measurements of sediment transport under sheet flow conditions. In: Proceedings of Coastal Sediments '03. Clearwater FL.

Li, M., Pan, S., O'Connor, B.A., 2008. A two-phase numerical model for sediment transport prediction under oscillatory sheet flows. Coastal Engineering 55, 1159–1173.

Liu, H., Sato, S., 2006. A two-phase flow model for asymmetric sheetflow conditions. Coastal Engineering 53 (10), 825–843.

Malarkey, J., Davies, A.G., Li, Z., 2003. A simple model of unsteady sheet flow sediment transport. Coastal Engineering 48 (3), 171–188.

McLean, S.R., Ribberink, J.S., Dohmen-Janssen, C.M., Hassan, W.N., 2001. Sand transport in oscillatory sheet flow with mean current. Journal of Waterway, Port, Coastal and Ocean Engineering 127 (3), 141–151.

O'Donoghue, T., Wright, S., 2004a. Concentrations in oscillatory sheet flow for well sorted and graded sands. Coastal Engineering 50 (3), 117–138.

O'Donoghue, T., Wright, S., 2004b. Flow tunnel measurements of velocities and sand flux in oscillatory sheet flow for well sorted and graded sands. Coastal Engineering 51, 1163–1184.

Osborne, P.D., Vincent, C.E., 1993. Dynamics of large and small scale bedforms on a macrotidal shoreface under shoaling and breaking waves. Marine Geology 115, 207–226.

Ribberink, J.S., Al-Salem, A.A., 1995. Sheet flow and suspension of sand in oscillatory boundary layers. Coastal Engineering 25 (3–4), 205–225.

Rose, C.P. et al., 1999. Vertical sediment entrainment characteristics in Oscillatory sheet flow conditions. In: Proceedings of Coastal Sediments '99. Long Island NY, USA, pp. 135–147.

Wilson, K.C., 1989. Mobile-bed friction at high shear stress. Journal of Hydraulic Engineering 115 (6), 825–830.

Wright, S., O'Donoghue, T., 2002. Oscillatory flow tunnel experiments at Aberdeen University. EPSRC LUBA Report, University of Aberdeen, Department of Engineering, Aberdeen.

Zara Flores, N., Sleath, J.F.A., 1998. Mobile layer in oscillatory sheet flow. Journal of Geophysical Research 103 (C6), 12783–12793.